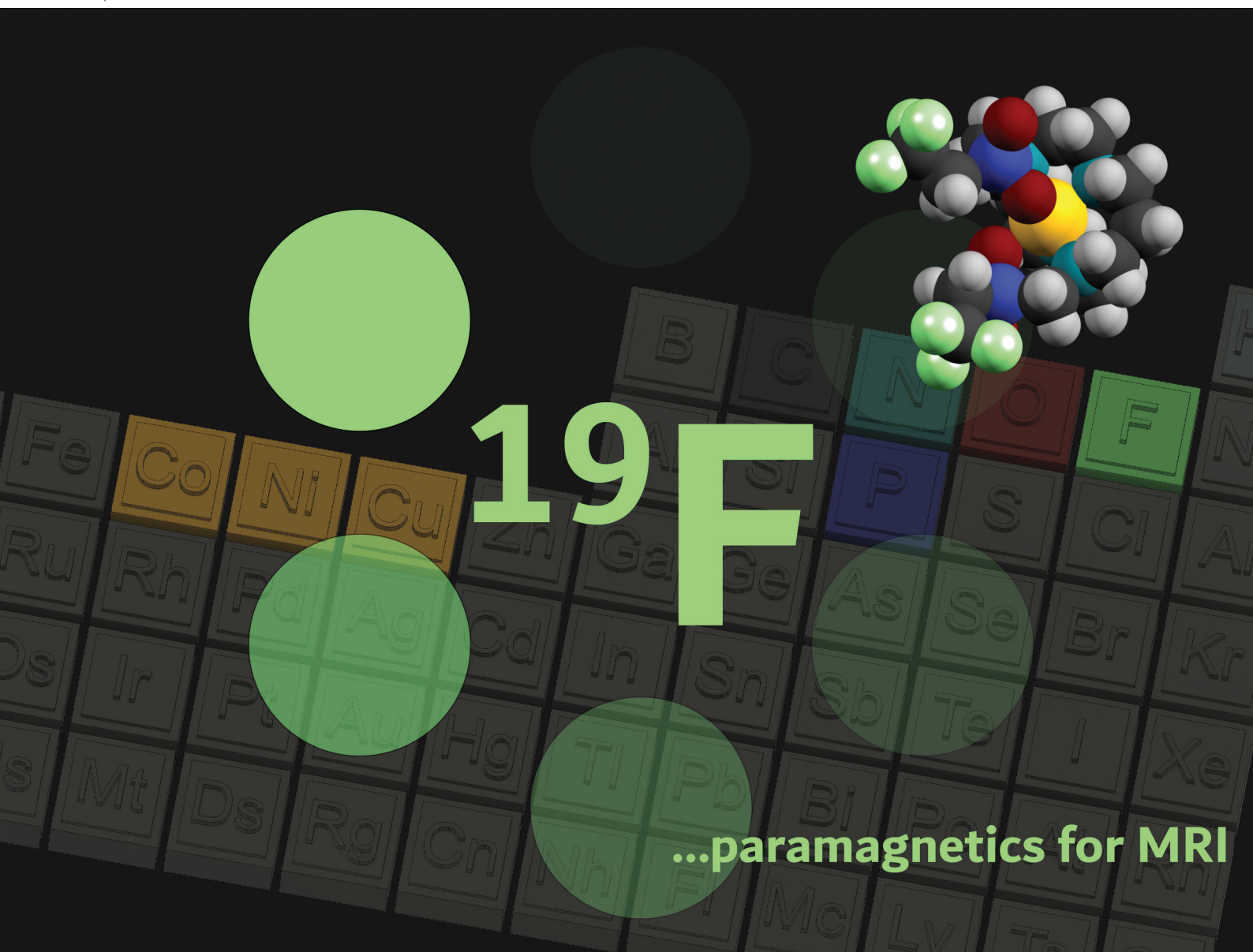


Dalton Transactions

An international journal of inorganic chemistry

rsc.li/dalton






ISSN 1477-9226

PAPER

Jan Kotek *et al.*

Transition metal complexes of cyclam with two
2,2,2-trifluoroethylphosphinate pendant arms as probes for
 ^{19}F magnetic resonance imaging

Cite this: *Dalton Trans.*, 2023, **52**, 12208Transition metal complexes of cyclam with two 2,2,2-trifluoroethylphosphinate pendant arms as probes for ^{19}F magnetic resonance imaging†Filip Koucký, Jan Kotek, * Ivana Císařová, Jana Havlíčková, Vojtěch Kubiček  and Petr Hermann 

A new cyclam-based ligand bearing two methylene(2,2,2-trifluoroethyl)phosphinate pendant arms was synthesized and its coordination behaviour towards selected divalent transition metal ions [Co(II), Ni(II), Cu(II), Zn(II)] was studied. The ligand was found to be very selective for the Cu(II) ion according to the common Williams–Irving trend. Complexes with all the studied metal ions were structurally characterized. The Cu(II) ion forms two isomeric complexes; the pentacoordinated isomer *pc*-[Cu(L)] is the kinetic product and the octahedral *trans*-*O,O'*-[Cu(L)] isomer is the final (thermodynamic) product of the complexation reaction. Other studied metal ions form octahedral *cis*-*O,O'*-[M(L)] complexes. The complexes with paramagnetic metal ions showed a significant shortening of ^{19}F NMR longitudinal relaxation times (T_1) to the millisecond range [Ni(II) and Cu(II) complexes] or tens of milliseconds [Co(II) complex] at the temperature and magnetic field relevant for ^{19}F magnetic resonance imaging (MRI). Such a short T_1 results from a short distance between the paramagnetic metal ion and the fluorine atoms (~6.1–6.4 Å). The complexes show high kinetic inertness towards acid-assisted dissociation; in particular, the *trans*-*O,O'*-[Cu(L)] complex was found to be extremely inert with a dissociation half-time of 2.8 h in 1 M HCl at 90 °C. Together with the short relaxation time, it potentially enables *in vitro/in vivo* utilization of the complexes as efficient contrast agents for ^{19}F MRI.

Received 12th May 2023,
Accepted 7th June 2023

DOI: 10.1039/d3dt01420g

rsc.li/dalton

Introduction

Among diagnostic techniques, magnetic resonance imaging (MRI) plays a crucial role in modern medicine. Its main advantage comes from the use of non-ionizing radiation, compared to classical radiomedicinal methods such as computed tomography (CT), single-photon emission computed tomography (SPECT) and positron emission tomography (PET) where ionizing radiation is used. However, MRI suffers from much lower sensitivity compared to SPECT and PET. Classical MRI detects an NMR effect of water ^1H nuclei where sensitivity and image contrast can be improved by the application of so-called contrast agents (CAs). These compounds influence proton relaxation times (longitudinal, T_1 , and transversal, T_2) of water

molecules present in their vicinity, and the use of an appropriate pulse sequence increases or decreases the water ^1H signals of the given tissue selectively.¹ In addition, modern MRI techniques can also detect ^1H signals of other compounds present in the organism (*e.g.* fat). Furthermore, the use of responsive (“smart”) contrast agents which modulate their response according to surrounding conditions can provide information on the physiological status of tissues.² Alternatively, NMR spectra of parts of tissues could be acquired by a method called magnetic resonance spectroscopy imaging (MRSI).³ Also other NMR active nuclei such as ^{13}C , ^{19}F or ^{31}P can be detected by MRI.^{4,5} Among them, ^{19}F is of special interest as its gyromagnetic momentum is close to that of ^1H which enables detection of ^{19}F NMR signals on proton MRI scanners with only small hardware and software modifications. Furthermore, fluorine is a monoisotopic element and has almost no abundance in living organisms which predisposes it for use in “hot-spot” imaging. The need for “hot-spots” overlaid with anatomical images can be elegantly solved by $^1\text{H}/^{19}\text{F}$ MRI tandem imaging on the same hardware. Such an imaging method could be particularly useful *e.g.* in monitoring the fate of transplanted cells (cell tracking).^{6–8}

A number of compounds have been tested as ^{19}F NMR contrast agents. They were usually perfluorinated hydrocarbons

Department of Inorganic Chemistry, Faculty of Science, Charles University, Hlavova 8, 128 42 Prague 2, Czech Republic. E-mail: modrej@natur.cuni.cz

† Electronic supplementary information (ESI) available: NMR spectra of studied complexes, colour change of isomeric Cu(II) complexes, experimental data and details for the crystal structure refinement, ligand distribution diagram, details of the kinetic inertness study, NMR characterization of organic compounds, and discussion of the crystal structures of synthetic intermediates. CCDC 2262037–2262048. For ESI and crystallographic data in CIF or other electronic format see DOI: <https://doi.org/10.1039/d3dt01420g>



and their derivatives (for simplicity, they are called perfluorocarbons, PFCs), and some of them have been already studied for a long time as potential blood substitutes.^{9,10} The list of compounds includes *e.g.* hexafluorobenzene,¹¹ perfluorodecalin,¹² tris(perfluoroalkyl)amines,¹³ perfluorinated crown ethers,^{14–18} fluorinated polymers,¹⁹ *etc.*, which are used in the form of nanoemulsions. However, these organic compounds show very long T_1 relaxation times. Therefore, a long delay between excitation pulses is needed, which prolongs the total acquisition time. To shorten the time of imaging, complexes of fluorine-containing ligands with paramagnetic metal ions were introduced.^{20–22} They are usually complexes of lanthanide (III) ions [with a generally large magnetic momentum, especially for Dy(III) and Ho(III)] with ligands based on a cyclen (1,4,7,10-tetraazacyclododecane) skeleton (*e.g.* H₄dota derivatives, Fig. 1),^{23,24} which ensures kinetic inertness of these contrast agents.^{25,26} More recently, transition metal ion complexes have been also found to effectively shorten T_1 relaxation times.^{27–30} Here, especially complexes of cyclam-based ligands (cyclam = 1,4,8,11-tetraazacyclotetradecane, Fig. 1) were found to be promising.^{31–36} In general, the cyclam derivatives are not suitable for complexation of lanthanide ions due to an inappropriately large macrocyclic cavity, but they are well known for effective binding of heavier first-row transition metal ions. In particular, Cu(II) and Ni(II) ions are bound very selectively into thermodynamically stable and kinetically inert complexes.^{37–41} However, some Ni(II) complexes of 1,8-bis(2,2,2-trifluoroethyl)-cyclam derivatives (1,8-tfe₂cyclams, Fig. 1) showed decreased stability and kinetic inertness, and have in general very short relaxation times (in the millisecond range) due to a very short distance between the paramagnetic centre and fluorine atoms, which prevents simple measurement and places non-trivial demands on the hardware used for imaging.³² In this respect, analogous Co(II) complexes with $T_1 \sim 10\text{--}15$ ms seem to be more promising.³⁴ In addition, we designed a series of ligands with larger separation of the fluorine atoms from the paramagnetic metal ion centre [1,8-(tfe-NHR)₂cyclams, Fig. 1].⁴² It was shown that complexation of Cu(II) to these structures shortens significantly fluorine relax-

ation times to an optimal range (order of tenths of milliseconds).⁴² Some time ago, we introduced (2,2,2-trifluoroethyl) phosphinic acid as a suitable pendant arm in the cyclen-based ligand H₄dotp^{tfe} (Fig. 1) and studied its lanthanide(III) complexes.⁴³ To extend our work in this field, we report on the results of our study of a new cyclam derivative with two (2,2,2-trifluoroethyl)phosphinic acid pendant moieties in the 1,8-positions (H₂L, Fig. 1).

Experimental

General

Commercial chemicals (Fluka, Aldrich, CheMatech, Lachema, Fluorochem) were used as obtained. Anhydrous solvents were obtained by established procedures⁴⁴ or purchased. The 1,8-dibenzyl-cyclam **1** was prepared by the reported procedure.⁴⁵

Thin-layer chromatography (TLC) was performed on silica-coated aluminium sheets, silica gel 60 F254 (Merck). Spots were visualized using UV light (254 and 366 nm), spraying with 0.5% ethanolic solution of ninhydrin, and dipping in 5% aq. solution of CuSO₄, iodine vapour or in aq. solution of 1% KMnO₄ and 2% Na₂CO₃.

NMR spectra were recorded on NMR spectrometers Varian VNMRS300 equipped with a pseudo-4-channel probe (frequencies 299.9 MHz for ¹H, 282.2 MHz for ¹⁹F and 121.4 MHz for ³¹P), Varian Inova 400 MHz (frequencies 400.0 MHz for ¹H, 100.6 MHz for ¹³C, 376.3 MHz for ¹⁹F and 161.9 MHz for ³¹P) equipped with an ID-PFG probe for ¹⁹F relaxation experiments or with an ASW 4NUC probe, or Bruker Avance III 600 MHz (frequencies 600.2 MHz for ¹H, 150.9 MHz for ¹³C and 564.7 MHz for ¹⁹F) equipped with a cryoprobe (¹H, ¹³C, ¹⁵N) or with a BBO probe (¹⁹F). Representative NMR spectra of the prepared compounds are given in the ESI.† The spectra were acquired at 25 °C unless stated otherwise. Internal references for ¹H and ¹³C NMR spectra were *t*-BuOH for D₂O solutions and the CHD₂OD residual peak for MeOH-*d*₄ solutions, respectively. Aq. H₃PO₄ (3%) was used as the external reference for ³¹P NMR, and *ca.* 1% triflic acid for ¹⁹F NMR. These sec-

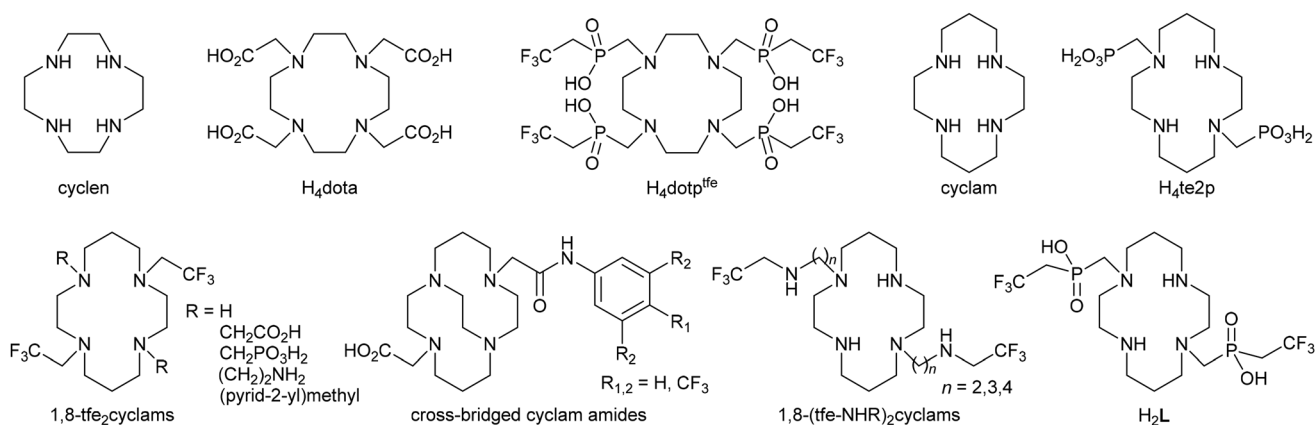


Fig. 1 Ligands mentioned in the text.



ondary references were referenced to 85% H_3PO_4 (0.0 ppm) and to Freon-11 (0.0 ppm) respectively. Chemical shifts are given in ppm and coupling constants at Hz. Chemical shifts of paramagnetic compounds were corrected for the bulk magnetic susceptibility effect: to the sample, a small amount of 2,2,2-trifluoroethanol was added, and the chemical shift was measured using an insert cuvette containing the secondary reference. The same insert cuvette was used to measure the chemical shift of 2,2,2-trifluoroethanol in a pure solvent, and the difference between the signals of trifluoroethanol was used for chemical shift correction of the paramagnetic compound. The T_1 relaxation times of the ^{19}F NMR signal were measured with the inversion recovery sequence. The T_2 relaxation times of diamagnetic compounds were measured with the CPMG sequence on Varian Inova 400 MHz and Bruker III 600 MHz; the measurement is not accessible on VNMR300 as the probe used does not provide accurate 180° pulses for ^{19}F nuclei. The T_2^* relaxation times were calculated for all paramagnetic complexes from half-widths of the NMR signals.

Mass spectra were recorded on a Waters ACQUITY QDa, which is a part of the Waters Arc HPLC system. Data were processed using Empower 3 software. Samples were dissolved in water, MeOH or MeCN. The HPLC was run on the same device using the Cortecs C18 2.7 μm , 4.6×50 mm column and $\text{H}_2\text{O}:\text{MeCN}$ 100 to 0% gradient [0.1% trifluoroacetic acid (tfa) used as a modifier].

The UV-Vis spectra were recorded on a spectrometer Specord 50 Plus (Analytic Jena) in a quartz-glass cell with an optical path of 1 cm in the range of 350–1100 nm.

Ligand synthesis

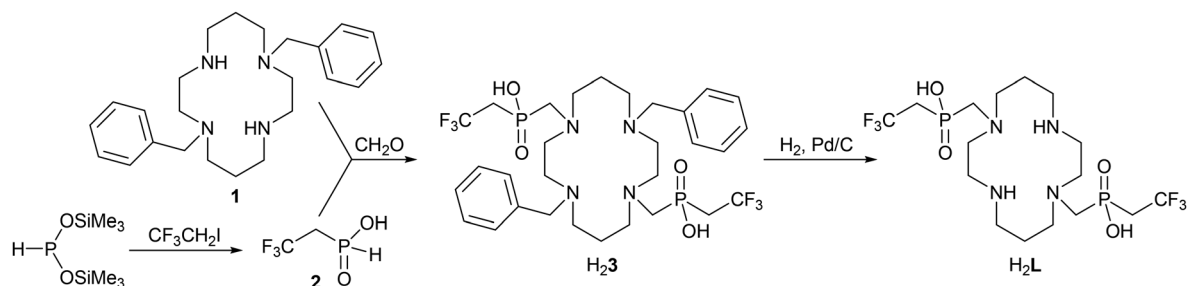
Synthesis of the studied ligand was performed according to Scheme 1.

(2,2,2-Trifluoroethyl)phosphinic acid, 2. Dry solid hypophosphorous acid (7.6 g, 106 mmol) was placed into a 250 ml three-necked round-bottom flask containing a stirring bar. The flask was equipped with an argon inlet, a spiral cooler with a Nujol bubble-counter and a septum, and was thoroughly flushed with argon. Further procedures were performed under a gentle stream of Ar. Solid H_3PO_2 was dissolved in anhydrous dichloromethane (DCM, 50 ml) and added through the septum. The flask was immersed in a water cooling bath (room temperature) and anhydrous *N,N*-diisopropylethylamine (DIPEA, 41.1 g, 318 mmol, 3.0 equiv.) was added through the septum. Afterwards, trimethylsilyl chloride (TMSCl, 34.5 g, 318 mmol, 3.0 equiv.) was added dropwise; the rate of addition was slow to prevent the white haze formed from flowing away with the Ar stream from the apparatus. After the addition of the entire amount of TMSCl, the reaction mixture was stirred at room temperature for 3 h. The ^{31}P NMR spectrum of the reaction mixture shows quantitative formation of $\text{HP}(\text{OTMS})_2$ (δ 140.9 ppm, d, $^1J_{\text{PH}}$ 177 Hz). After this period, 2,2,2-trifluoroethyl iodide (26.6 g, 116 mmol, 1.1 equiv.) dissolved in anhydrous DCM (20 ml) was added dropwise into the reaction mixture; the rate of addition was chosen to prevent the white haze formation and overheating (boiling) of the mixture. The mixture was stirred at room temperature for 15 h. The reaction mixture was then hydrolysed/alcoholysed by slow addition of 96% aq. EtOH (250 ml) and the ^{31}P NMR of the hydrolysed mixture was acquired – besides the product (14.5 ppm, dm, $^1J_{\text{PH}}$ 576 Hz, conversion $\sim 70\%$) and its ethyl ester (23.1 ppm, dm, $^1J_{\text{PH}}$ 590 Hz, conversion $\sim 10\%$), H_3PO_3 (1.8 ppm, d, $^1J_{\text{PH}}$ 660 Hz, $\sim 20\%$) was also present as the main by-product.

The volatiles were evaporated on a rotary evaporator at a bath temperature of 50°C . The remaining material was poured onto a column of a strong cation exchange resin in a H^+ -cycle (Dowex 50, 500 ml) and the mixture of acids was eluted with water (DIPEA was retained on the column). Acid fractions were concentrated on a rotary evaporator at 40°C . The ^1H NMR spectrum confirmed the absence of DIPEA in the eluted material. After this procedure, ethyl ester of 2 present in the initial mixture was completely hydrolysed.

A solution of $\text{Pb}(\text{OAc})_2$ in 20% acetic acid (1 M, 70 ml) was added into the evaporated eluate obtained above and diluted with water (50 ml). The mixture was stirred at room temperature for 3 h and the yellow precipitate of PbI_2 was removed by filtration on a Büchner funnel through several layers of filtration paper. Excess $\text{Pb}(\text{II})$ in the filtrate was removed by bubbling hydrogen sulphide through the solution and the PbS precipitate was filtered off using a Büchner funnel with a paper mesh. Volatiles from the filtrate were removed at 50°C using a rotary evaporator.

The product was purified on a silica column (300 ml) using conc. aq. $\text{NH}_3:\text{EtOH}$ 1:20 as a mobile phase [$R_f(\text{product})$ 0.65, $R_f(\text{H}_3\text{PO}_3)$ 0.35]. Fractions containing the pure product



Scheme 1 Synthesis of ligand H_2L .



were combined and evaporated giving the ammonium salt of (2,2,2-trifluoroethyl)phosphinic acid as a white solid. Free acid was obtained by passing a solution of the ammonium salt through a column of a strong cation exchange resin (Dowex 50, H⁺-form, 100 ml, elution with water) and evaporation of the eluate at 40 °C. Yield 9.0 g (57%) as a clear colourless oil.

NMR (ammonium salt, D₂O, pD 4.6). ¹H: 7.15 (d; 1H; HP; ¹J_{HP} 547), 2.63 (m; 2H; CH₂). ¹³C{¹H}: 37.5 (dq; CH₂; ²J_{CF} 27.3, ¹J_{CP} 81.3), 125.8 (qd; CF₃; ¹J_{CF} 275; ²J_{CP} 3.1). ¹⁹F: -57.7 (pseudo-q; ³J_{FH} ≈ ³J_{FP} ≈ 12.0). ³¹P{¹H}: 13.3 (q, ³J_{PF} 12.0). ³¹P: 13.3 (dm, ¹J_{PH} 547). MS-ESI, (+): 149.0 [M + H]⁺; (-): 146.7 [M - H]⁻. TLC (conc. aq. NH₃:EtOH 1:20); R_f 0.65 (ninhydrin, yellow spot; KMnO₄/Na₂CO₃, yellow spot).

4,11-Dibenzyl-1,8-bis{[(2,2,2-trifluoroethyl)(hydroxy)phosphoryl]methyl}-1,4,8,11-tetraazacyclotetradecane, H₂3. The 1,8-dibenzyl-cyclam tetrahydrochloride tetrahydrate (1·4HCl·4H₂O, 0.60 g, 1.0 mmol) was dissolved in water (20 ml) and the solution was mixed with 10% aq. NaOH (20 ml). Free **1** was extracted with DCM (2 × 50 ml) and the organic phase was evaporated. Free amine **1** was dissolved in 50% (v/v) aq. trifluoroacetic acid (tfa, 20 ml). To this solution, a solution of (2,2,2-trifluoroethyl)phosphinic acid **2** (1.3 g, 8.8 mmol, 8.8 equiv.) in 50% (v/v) aq. tfa (20 ml) was added. Paraformaldehyde (0.11 g, 3.6 mmol, 3.6 equiv.) was added and the flask was closed with a stopper. The reaction mixture was stirred at 60 °C for 12 h. After this time, a new amount of paraformaldehyde (0.40 g, 13 mmol, large excess) was added and the mixture was stirred at 60 °C for 24 h. After this period, a new amount of paraformaldehyde (0.40 g, 13 mmol) was added again and the mixture was stirred at 60 °C for another 24 h. The ³¹P NMR spectrum showed the disappearance of the starting phosphinic acid **2** (no signal of a compound containing P-H bonds was found in the spectra). During the course of the reaction, the crude product precipitated off in the reaction mixture. The crude product was filtered off from the cold reaction mixture and recrystallized from boiling 50% (v/v) aq. tfa (50 ml per 1.0 g of the crude product). Recrystallization afforded white needle-like crystals; a single crystal suitable for the X-ray diffraction study was selected from the bulk. Crystals of H₂3·6CF₃CO₂H·2H₂O were isolated by filtration (0.96 g, 68%). Compound H₂3 can also be obtained as zwitterionic H₂3·6H₂O after repeated recrystallization in boiling water. Such a procedure afforded colourless crystals of H₂3·6H₂O suitable for X-ray diffraction analysis.

EA (H₂3·6CF₃CO₂H·2H₂O): found (calc. for C₄₂H₅₄F₂₄N₄O₁₈P₂, M_r 1420.81) C: 35.68 (35.51), H: 3.60 (3.83), N: 3.73 (3.94), F: 31.28 (32.09), P: 4.13 (4.36). NMR (H₂3·6H₂O, MeOH-*d*₄, atom numbering scheme is given in the ESI[†]). ¹H: 2.11–2.30 (4H, m, H6); 2.33–2.40 (2H, m, H2); 2.43–2.58 (6H, m, H9 and H8); 2.60–2.67 (2H, m, H8); 2.78–2.86 (4H, m, H5 and H7); 2.91–3.01 (4H, m, H3 and H7); 3.26–3.34 (1H, m, H3); 3.34–3.41 (2H, m, H2); 3.68–3.74 (2H, m, H5); 4.21–4.27 (2H, m, H11); 4.39–4.46 (2H, m, H11); 7.47–7.53 (6H, m, H14 and H15); 7.56–7.61 (4H, m, H13). ¹³C{¹H}: 24.56 (s, C6); 37.32 (dq, C9, ²J_{CP} 79.6, ²J_{CF} 28.2); 49.9 (s, C2); 50.3 (s, C5); 52.0 (s, C3); 54.9 (d, C8, ²J_{CP} 119); 58.5 (s, C7); 58.8 (s, C11); 127.8 (q, C10,

¹J_{CF} 275.1 Hz); 130.8 (s, C12); 131.1 (s, C14); 131.9 (s, C15); 134.1 (s, C13). ¹⁹F: -58.06 (dt; ³J_{FH} 12.3, ³J_{FP} 6.8). ³¹P{¹H}: 23.4 (q, ³J_{PF} 6.9). ³¹P: 23.5 (m). MS-ESI, (+): 701.4 [M + H]⁺; (-): 699.4 [M - H]⁻. TLC (conc. aq. NH₃:EtOH 1:10); R_f 0.80 (CuSO₄, green spot).

1,8-Bis{[(2,2,2-trifluoroethyl)(hydroxy)phosphoryl]methyl}-1,4,8,11-tetraazacyclotetradecane, H₂L. Compound H₂3·6CF₃CO₂H·2H₂O (570 mg, 0.40 mmol) was dissolved in 90% aq. AcOH (15 ml) in a 50 ml pear-shaped flask and 10% Pd/C catalyst (130 mg) was added under an Ar atmosphere. The flask was flushed with H₂ and the reaction mixture was stirred under a H₂ atmosphere (balloon) for 24 h. The catalyst was filtered off and all volatiles were evaporated. The remaining solid was re-dissolved in 90% aq. AcOH and the solution was evaporated again, yielding an oily residue, which crystallized upon standing (245 mg, 80%). Single crystals of H₂L·4AcOH suitable for X-ray diffraction analysis were selected from the bulk. The acetic acid adduct was dissolved in boiling water (~3 ml) and the same volume of conc. aq. HCl was added. Upon cooling, the solid phase of the composition (H₆L)Cl₄·4H₂O was isolated (190 mg, 65% with respect to H₂3·6CF₃CO₂H·2H₂O). A sample of this material was dissolved in hot water, and single crystals of the composition (H₄L)Cl₂·4H₂O suitable for diffraction measurement were formed upon slow concentration at room temperature.

EA [(H₆L)Cl₄·4H₂O]: found (calc. for C₁₆H₄₄Cl₄F₆N₄O₈P₂ M_r 738.29) C: 27.07 (26.03), H: 5.30 (6.01), N: 7.94 (7.59), F: 15.63 (15.44), P: 8.16 (8.39), Cl: 19.36 (19.21). NMR [(H₆L)Cl₄·4H₂O, D₂O, pD 9.0 (NaOD), atom numbering scheme is given in the ESI[†]). ¹H: 1.97 (4H, bs, H6); 2.72 (4H, pseudo-p, ³J_{HF} ≈ ³J_{HP} ≈ 12.4, H9); 2.85 (4H, bs, H2 and H8); 2.92 (8H, bs, H2 and H7); 3.12 (4H, bs, H3); 3.21 (4H, t, ³J_{HH} 5.9, H5). ¹³C{¹H}: 24.1 (s, C6); 35.1 (dq, C9, ¹J_{CP} 79.5, ²J_{CF} 28.6); 45.9 (s, C3); 48.2 (s, C5); 54.5 (d, C8, ¹J_{CP} 117.3); 55.4 (d, C2, ³J_{CP} 6.6); 58.8 (d, C7, ³J_{CP} 5.5); 125.7 (qd, C10, ¹J_{CF} 274.9, ²J_{CP} 3.2). ¹⁹F: -57.34 (dt; ³J_{FH} 12.0, ³J_{FP} 7.2). ³¹P{¹H}: 28.5 (q, ³J_{PF} 7.3). ³¹P: 28.5 (m). MS-ESI, (+): 521.2 [M + H]⁺, 1041.5 [2M + H]⁺. TLC (conc. aq. NH₃:EtOH 1:5); R_f 0.80 (CuSO₄, violet spot).

Preparation of complexes of H₂3

Mixing H₂3·6CF₃CO₂H·2H₂O (50 mg) with Cu(OAc)₂·H₂O (8 mg, 1.1 equiv.) in water:MeOH (1:1, 2 ml) and neutralization with 2% aq. LiOH afforded an emerald green precipitate of the *pc*-[Cu(3)] complex which is only sparingly soluble in alcohols. A few green single crystals were isolated after the concentration of the mother liquor and acetone vapour diffusion. The X-ray structural analysis of these crystals revealed the composition as *pc*-[Cu(3)]-Cu(AcO)_{1.8}(tfa)_{0.2}·4H₂O·0.5acetone.

Attempts to prepare complexes of H₂3 with Co(II), Ni(II) and Zn(II) by mixing H₂3 with MCl₂ in aq. MeOH solutions and addition of aq. ammonia as a base led to the formation of precipitates insoluble in all common solvents (H₂O, MeOH, EtOH, DMSO, DMF, CHCl₃).

Preparation of complexes of H₂L

cis-O,O'-[Co(L)], *cis*-O,O'-[Ni(L)] and isomeric mixture of [Zn(L)]. Hydrochloric acid-free stock solutions of H₂L were pre-



pared using a strong cation exchange resin. The solution of $(\text{H}_6\text{L})\text{Cl}_4 \cdot 4\text{H}_2\text{O}$ (350 mg) in water (5 ml) was poured onto a column of the resin (Dowex 50, H^+ -form, 10 ml). The column was washed with water to neutrality of an eluate, and the free ligand was eluted using 5% aq. ammonia. The eluate was evaporated to dryness, and repeatedly dissolved in a small amount of water and evaporated again to remove NH_3 . The residue was dissolved in water (10 ml) and the concentration of H_2L (46.0 mM) was determined by ^{19}F qNMR with respect to the standardized aq. solution of tfa.

Solutions of complexes for ^{19}F NMR characterization were prepared directly in the NMR tube by mixing 150 μl of 18.4 mM solution of $(\text{H}_6\text{L})\text{Cl}_4 \cdot 4\text{H}_2\text{O}$ used for potentiometry, HEPES buffer (300 μl , 0.5 M, pH 7.4) and an appropriate volume of the solution of the metal salt (*ca.* 50 mM). The $\text{Zn}(\text{II})$ complex was prepared by mixing the ligand and a slight excess (1.2 equiv.) of ZnCl_2 to ensure the absence of free H_2L as, due to diamagnetism of the sample, the signal of free H_2L would be hardly distinguishable from the signal(s) of the complex isomers; it would complicate the interpretation of the NMR spectra. The $\text{Ni}(\text{II})$ and $\text{Co}(\text{II})$ complexes were prepared using a slightly sub-stoichiometric amount of $\text{Ni}(\text{NO}_3)_2$ or $\text{Co}(\text{NO}_3)_2$, respectively. In these cases, the signal of the diamagnetic H_2L excess was used as an internal reference. For the $\text{Co}(\text{II})$ complex, the NMR tube was flushed with Ar and pH was increased to 8.0 with aq. NaOH to ensure the full complexation of $\text{Co}(\text{II})$ ions (according to the results of the potentiometric study, see below). The $\text{Co}(\text{II})$ complex showed one ^{19}F NMR signal (-38.6 ppm, Fig. S1 \dagger) which remained unchanged with further standing (only some negligible oxidation to diamagnetic $\text{Co}(\text{III})$ was observed if the tube was opened to air; a very small diamagnetic signal appeared); further study revealed its *cis-O,O'*-[Co(L)] geometry (see below). However, solutions containing $\text{Ni}(\text{II})$ and $\text{Zn}(\text{II})$ complexes showed complicated spectra. Therefore, the samples were equilibrated for several days at 80 $^\circ\text{C}$. The measured ^{19}F NMR spectra of the fully equilibrated solutions showed one major signal of the $\text{Ni}(\text{II})$ complex at -47.1 ppm ($\sim 80\%$) besides two minor signals at -43.7 and -47.7 ppm with equal intensity (each $\sim 10\%$), as shown in Fig. S2 \dagger . Based on a further ^{19}F NMR study, the *cis-O,O'*-[Ni(L)] geometry was suggested with *R/S* isomerism of the phosphorus atom (see below). In the case of the $\text{Zn}(\text{II})$ - H_2L system, an isomeric mixture of three complexes was observed (pseudo-quartets due to ^{19}F - ^{31}P / ^1H couplings centred at -57.15 ppm, $\sim 40\%$; -57.23 ppm, $\sim 55\%$; -57.30 ppm, $\sim 5\%$, Fig. S3 \dagger). In the case of the diamagnetic $\text{Zn}(\text{II})$ - H_2L system, it was possible to acquire the ^{31}P NMR spectra also, which were consistent with the ^{19}F NMR data (three signals in ^{31}P NMR spectra, 30.1 ppm, $\sim 55\%$; 29.4 ppm, $\sim 5\%$; 28.7 ppm, $\sim 40\%$, Fig. S4 \dagger). The same ^{19}F and ^{31}P NMR spectra were observed for several independently prepared samples of the [Zn(L)] complex after the equilibration.

An alternative way was used to prepare complex solutions without additional salts and excess ligand: a solution of H_2L (46.0 mM, 840 μl , *ca.* 20 mg of H_2L) was mixed with 1.5 equiv. of CoCO_3 (7 mg) or with freshly precipitated $\text{M}(\text{OH})_2$ excess

[$\text{M} = \text{Ni}, \text{Zn}$ prepared by the addition of aq. LiOH to aq. MCl_2 (2.0 equiv.) and washing the precipitate with water by repeated centrifugation]. The mixtures were stirred in a closed vial at 80 $^\circ\text{C}$ for 5 d. After cooling, the excess of the solid phase was filtered off and the filtrate was concentrated. The measured ^{19}F NMR spectra confirmed the absence of free H_2L and showed the same signals of the complexes as found in the samples mentioned above, including the same ratio of the isomeric species.

The formation of the complexes was confirmed also by mass spectrometry. MS-ESI, (+): [Co(L)]: 578.2 [$^{59}\text{CoL} + \text{H}$] $^+$; 577.2, [^{59}CoL] $^+$; [Ni(L)]: 577.1 [$^{58}\text{NiL} + \text{H}$] $^+$; [Zn(L)]: 583.2 [$^{64}\text{ZnL} + \text{H}$] $^+$.

Single crystals of *cis-O,O'*-[Co(L)] $\cdot\text{LiCl}\cdot 3\text{H}_2\text{O}$ were prepared by acetone vapour diffusion into a solution of the complex prepared from a mixture of H_2L and CoCl_2 neutralized with LiOH.

Single crystals of *cis-O,O'*-[Ni(L)] $\cdot 3.5\text{H}_2\text{O}$ and *cis-O,O'*-[Zn(L)] $\cdot 2\text{H}_2\text{O}\cdot 0.5\text{acetone}$ were formed on acetone vapour diffusion into solutions of the corresponding complexes prepared from $\text{M}(\text{OH})_2$ as described above.

***pc*-[Cu(L)].** A blue solution of *pc*-[Cu(L)] for ^{19}F NMR characterization was prepared directly in the NMR tube by mixing 18.4 mM solution of $(\text{H}_6\text{L})\text{Cl}_4 \cdot 4\text{H}_2\text{O}$ (150 μl), formate buffer (0.5 M, pH 4.0, 300 μl) and 50.2 mM CuCl_2 (50 μl , 0.9 equiv.) at room temperature. The TLC analysis showed the exclusive formation of the *pc*-[Cu(L)] isomer. The measured ^{19}F NMR spectra showed (besides the signal of the ligand excess) one broad unsymmetrical signal of the *pc*-[Cu(L)] (~ -53 ppm, Fig. S5 \dagger). The signal can be deconvoluted into two broad peaks of approximately equal intensity (565 MHz: -52.6 ppm, $\nu_{\frac{1}{2}} \approx 500$ Hz; -53.2 ppm, $\nu_{\frac{1}{2}} \approx 400$ Hz, Fig. S5 \dagger).

Alternatively, 46.0 mM solution of H_2L (840 μl , *ca.* 20 mg of H_2L) was mixed with freshly precipitated $\text{Cu}(\text{OH})_2$ prepared by addition of 2% aq. LiOH to aq. solution of $\text{CuCl}_2 \cdot 2\text{H}_2\text{O}$ (13 mg, 2.0 equiv.) and washing the precipitate with water by repeated centrifugation. The mixture was stirred in a closed vial at room temperature overnight. The excess of $\text{Cu}(\text{OH})_2$ was filtered off and the filtrate was concentrated. The TLC analysis showed exclusive formation of the *pc*-[Cu(L)] isomer. The measured ^{19}F NMR spectra confirmed the absence of free H_2L and presence of the signal belonging to the *pc*-[Cu(L)] complex as mentioned above. TLC (conc. aq. NH_3 :EtOH 2:3): R_f 0.80 (blue spot, Fig. S7 \dagger). MS-ESI: (+): 581.9 [$\text{M} + \text{H}$] $^+$, 603.9 [$\text{M} + \text{Na}$] $^+$.

Single crystals of *pc*-[Cu(L)] $\cdot 3\text{H}_2\text{O}$ were formed on acetone vapour diffusion into a concentrated aqueous solution of the complex.

***trans-O,O'*-[Cu(L)].** The violet solution of *trans-O,O'*-[Cu(L)] for ^{19}F NMR characterization was prepared directly in the NMR tube by mixing 18.4 mM solution of $(\text{H}_6\text{L})\text{Cl}_4 \cdot 4\text{H}_2\text{O}$ (150 μl), HEPES buffer (0.5 M, pH 7.4, 300 μl) and 50.2 mM CuCl_2 (50 μl , 0.9 equiv.) at room temperature. The TLC spot of the *pc*-complex disappeared at 80 $^\circ\text{C}$ after 5 d. The measured ^{19}F NMR spectra showed (besides the signal of the ligand excess) one broad symmetrical signal of *trans-O,O'*-[Cu(L)] (565 MHz: -52.7 ppm, $\nu_{\frac{1}{2}} \approx 200$ Hz, Fig. S6 \dagger).

Alternatively, 46.0 mM solution of H_2L (1.25 ml, *ca.* 30 mg of H_2L) and $\text{CuCl}_2 \cdot 2\text{H}_2\text{O}$ (10 mg, 1 equiv.) was neutralized to



pH 7.4 with LiOH and heated at 90 °C for 5 d. The volatiles were evaporated and the complex was purified by chromatography on silica using conc. aq. NH₃:EtOH 2:3 as a mobile phase. The violet-coloured fraction was evaporated to dryness. The measured ¹⁹F NMR spectra confirmed the absence of free ligand and presence of one signal of the *trans*-Cu(II)-complex. TLC (conc. aq. NH₃:EtOH 2:3): R_f 0.95 (violet spot, Fig. S7†). MS-ESI: (+): 581.9 [M + H]⁺, 603.9 [M + Na]⁺.

Single crystals of *trans*-O,O'-[Cu(L)]·NH₄(Cl_{0.54}Br_{0.46}) were formed on acetone vapour diffusion into concentrated chromatographic fractions containing the complex.

Single crystals of *trans*-O,O'-[Cu(L)]·(H₃O)(ClO₄)·H₂O were crystallized by cooling of the saturated solution of the complex in boiling 1 M HClO₄.

Single-crystal X-ray diffraction study

The selected crystals were mounted on a glass fibre in a random orientation and the diffraction data were collected by using a Nonius KappaCCD diffractometer equipped with a Bruker APEX-II CCD detector using Mo-K_α radiation (λ = 0.71073 Å) at 150 K (Cryostream Cooler, Oxford Cryosystem) {H₂·3·6H₂O, H₂L·4AcOH and *cis*-O,O'-[Ni(L)]·3.5H₂O}, or with a Bruker D8 VENTURE Duo diffractometer with an IμS micro-focus sealed tube using Mo-K_α radiation at 150 K {*pc*-[Cu(3)]·Cu(AcO)_{1.8}(tfa)_{0.2}·4H₂O·0.5acetone, *pc*-[Cu(L)]·3H₂O and *trans*-O,O'-[Cu(L)]·NH₄(Cl_{0.54}Br_{0.46})} or at 120 K {H₂L·LiCl·6H₂O, *cis*-O,O'-[Co(L)]·LiCl·3H₂O, *trans*-O,O'-[Cu(L)]·(H₃O)(ClO₄)·H₂O, *cis*-O,O'-[Zn(L)]·2H₂O·0.5(C₃H₆O)}, or using Cu-K_α radiation (λ = 1.54178 Å) at 120 K [H₂·3·6CF₃CO₂H·2H₂O, (H₄L)Cl₂·4H₂O].

Data were analysed using the SAINT V8.34A–V8.40B software package (Bruker AXS Inc., 2015–2019). Data were corrected for absorption effects using the multi-scan method (SADABS).⁴⁶ All structures were solved by the direct methods (SHELXT2014)⁴⁷ and refined using full-matrix least-squares techniques (SHELXL2014).⁴⁸ Details on structure refinement are given in the ESI.†

All the data for the structures reported here have been deposited with the Cambridge Crystallographic Data Centre as supplementary publication numbers CCDC 2262037–2262048 (for an overview of experimental crystallographic data, see Table S1†).

Potentiometric study

The methodology of potentiometric titrations and processing of the experimental data were analogous to those previously reported.^{39,49} Titrations were carried out in a vessel tempered to 25 ± 0.1 °C at the ionic strength I = 0.1 M (NMe₄)Cl. The water ion product, pK_w = 13.81, and stability constants of M(II)–OH[−] systems were taken from the literature.⁵⁰

The ligand stock solution was prepared by the dissolution of (H₆L)Cl₄·4H₂O (1.3217 g) in a 100 ml volumetric flask. The solid (H₆L)Cl₄·4H₂O is slightly unstable due to the loss of HCl and water and, thus, the exact ligand concentration was determined by ¹⁹F qNMR (18.4 mM) using standardized aq. solution of tfa. This value agrees well with the value calculated

during the fitting of the protonation constants (difference < 1%). The overall protonation constants β_n are concentration constants and are defined by β_n = [H_nL]/([H]ⁿ·[L]) (stepwise protonation constants are defined as log K₁ = log β₁; log K_n = log β_n – log β_{n−1}). The overall stability constants are defined by the general equation β_{mlt} = [M_mH_nL_l]/([M]^m·[H]ⁿ·[L]^l). Here, the formation of only M:L = 1:1 complexes (m = l = 1) was suggested. The constants (with their standard deviations) were calculated with the OPIUM program.⁵¹ The protonation constants were determined using standard titrations in the pH range 1.6–12.1 with c_L = 0.004 M and starting volume approx. 5 ml (pH means “analytical” pH, −log[H⁺]). Equilibrium was established slowly in the metal(II)-containing systems. Therefore, stability constants of the complexes were obtained by the “out-of-cell” method. Each solution corresponding to one titration point of a common titration was prepared under an Ar stream in tubes with ground joints (pH 1.6–6.5, three titrations with 15 points) from the ligand, metal ion and HCl/(NMe₄)Cl stock solutions and water (starting volume ca. 1 ml, M:L molar ratio 0.95:1, c_L = 0.004 M). Then, a known amount of (NMe₄)OH standard solution was added under Ar. The tubes were firmly closed with stoppers and the solutions were left to equilibrate at room temperature. Afterwards, pH was measured with a freshly calibrated combined glass electrode in each tube. One set of tubes containing the Cu(II)–H₂L system was equilibrated for three weeks and the others for four weeks. Systems with Co(II), Ni(II) and Zn(II) were equilibrated for six weeks (one set of each metal ion) and eight weeks (the remaining sets). Identical results were obtained in both time points for each metal ion system proving a reaching the thermodynamic equilibrium after the shorter time period used.

Study of kinetic inertness of the complexes

The stock solution of the complex was mixed with water and stock solution of HCl to reach the final HCl concentration of 1.0 M in order to obtain dissociation data comparable with the related systems.³² The acid-assisted dissociation of Cu(II) complexes was followed by a decrease of their CT bands in the UV-Vis spectra (315 and 280 nm for the *pc*- and the *trans*-isomer, respectively); the temperature of the experiment was chosen to obtain data within a reasonable time (<~24 h): 25 °C and 90 °C for the *pc*- and the *trans*-isomer, respectively. Acid-assisted dissociation of the Co(II) and Ni(II) complexes was followed by ¹⁹F NMR (a decrease in the intensity of the signal of the complex, an increase in the intensity of the signal of the free ligand, and integrated with respect to tfa used as an external reference). Temperatures 25 °C and 90 °C were used for the Co(II) and the Ni(II) complexes, respectively.

Results and discussion

Synthesis of H₂L

Synthesis of the studied ligand was performed as shown in the Experimental section (Scheme 1).



The key starting compound, 2,2,2-trifluoroethylphosphinic acid **2**, was prepared by an Arbuzov-type reaction between 2,2,2-trifluoroethyl iodide and bis(trimethylsilyl)hypophosphite which was generated *in situ* from hypophosphorous acid and trimethylsilyl chloride in the presence of *N,N*-diisopropylethylamine (DIPEA) as a base. The silyl ester intermediate was hydrolysed with aqueous ethanol leading to the product **2** with conversion in the range of 60–80% (according to the intensity of the ^{31}P NMR signal (14.5 ppm, $^1J_{\text{PH}} = 576$ Hz) and phosphorous acid as a dominant by-product (1.8 ppm, $^1J_{\text{PH}} = 660$ Hz). Despite an excess of the alkylation agent used, no bis(2,2,2-trifluoroethyl)phosphinic acid was formed during the reaction, probably due to the low nucleophilicity of the monosubstituted derivative and volatility of the starting alkylation agent (Ar flow was used to ensure an inert atmosphere).

DIPEA was removed on a strong cation exchange resin in the H^+ -form and the acid eluate containing predominantly product **2**, phosphorous acid and hydroiodic acid was evaporated at $<40^\circ\text{C}$ (in bath) to avoid oxidation/disproportionation of product **2**. However, under such conditions, it was impossible to quantitatively remove HI. Any HI present in the crude product mixture forms elemental iodine on standing which oxidizes the compound **2** to 2,2,2-trifluoroethylphosphinic acid. HI was removed with an excess of lead(II) which was then precipitated by gaseous H_2S . The separation of product **2** and phosphorous acid was accomplished by chromatography on silica using aq. NH_3 :EtOH 1:20 as a mobile phase. After chromatography, the product was isolated in the form of a semi-solid ammonium salt. It was converted to free acid on a strong cation exchanger in the H^+ -form. Free acid **2** was isolated as a colourless oil in a moderate yield.

A Mannich-type reaction between 1,8-dibenzyl-cyclam **1**, 2,2,2-trifluoroethylphosphinic acid **2** and paraformaldehyde was performed in a strong acid solution (water:trifluoroacetic acid 1:1) at 60°C . Aq. HCl usually used as a solvent for this type of reaction cannot be used here due to the insolubility of the starting amine **1** in the solvent. In less acidic media (acetic acid), the reaction did not proceed even at 80°C but the oxidation of the P–H bond was observed instead. The product **H₂3** is insoluble in the reaction medium and was separated by filtration as an adduct with trifluoroacetic acid. Re-crystallization of the product from water:trifluoroacetic acid (1:1) afforded single crystals of $\text{H}_2\text{3}\cdot 6\text{CF}_3\text{CO}_2\text{H}\cdot 2\text{H}_2\text{O}$ suitable for X-ray diffraction analysis (see the ESI †). Despite the presence of several strong acid molecules in the solid-state structure, the macrocycle is only double-protonated and the protons are located on amino groups bearing the benzyl groups. Trifluoroacetic acid was removed by the re-crystallization of $\text{H}_2\text{3}\cdot 6\text{CF}_3\text{CO}_2\text{H}\cdot 2\text{H}_2\text{O}$ from water and $\text{H}_2\text{3}\cdot 6\text{H}_2\text{O}$ was obtained. Slow cooling of the saturated hot aq. solution afforded crystals suitable for the X-ray diffraction study (see the ESI †).

Debenzylation of the intermediate **H₂3** to **H₂L** was performed in 90% v/v aq. acetic acid under a H_2 atmosphere using Pd/C as a catalyst. After catalyst removal, ligand **H₂L** was isolated by the crystallization of the concentrated reaction

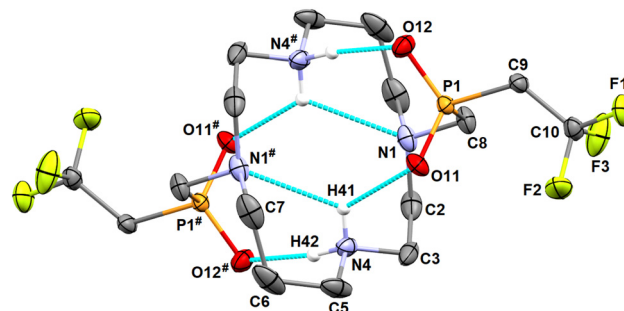


Fig. 2 Molecular structure of H_2L found in the crystal structure of $\text{H}_2\text{L}\cdot 4\text{AcOH}$. Carbon-bound hydrogen atoms are omitted for clarity. Intramolecular hydrogen bonds are shown as turquoise dashed lines. Selected centrosymmetry-related atoms are labelled with #.

mixture as a zwitterionic adduct with acetic acid $\text{H}_2\text{L}\cdot 4\text{AcOH}$. The procedure afforded single crystals of sufficient quality for the determination of the crystal structure. It revealed deprotonation of the phosphinate arms and protonation of the secondary amino groups, *i.e.* H_2L is present in a zwitterionic form (Fig. 2).

The zwitterionic molecule of H_2L possesses a centre of symmetry and adopts a “common” angular conformation similar to those found in the crystal structure of the cyclam itself and in its diprotonated forms.^{52,53} The phosphinate pendant arms are turned above/below the macrocyclic cavity and stabilize the molecular conformation by strong intramolecular hydrogen bonds [$d(\text{N}4\#\cdots\text{O}11) = 2.71 \text{ \AA}$, $d(\text{N}4\cdots\text{O}12) = 2.85 \text{ \AA}$]. Both molecules of the co-crystallized acetic acid are protonated and are bound by very strong hydrogen bonds to the phosphinate oxygen atoms [$d(\text{O}[\text{AcOH}]\cdots\text{O}11/\text{O}12) = 2.58 \text{ \AA}$, Fig. S21 †].

The ligand H_2L can be easily converted into hydrochloride (H_6L) $\text{Cl}_4\cdot 4\text{H}_2\text{O}$ by the crystallization of $\text{H}_2\text{L}\cdot 4\text{AcOH}$ from aq. HCl (6 M). Further re-crystallization of this material from water afforded (H_4L) $\text{Cl}_2\cdot 4\text{H}_2\text{O}$ which was structurally characterized. In the presence of HCl, all macrocycle amino groups of the ligand molecule are protonated which leads to the conformation (3,4,3,4)-D^{52,53} of the cyclam ring. The nitrogen atoms bearing the phosphinate pendant arms form the corners of the (3,4,3,4)-D rectangle (Fig. 3). Such a conformation maximizes the separation of the positive charges but avoids the for-

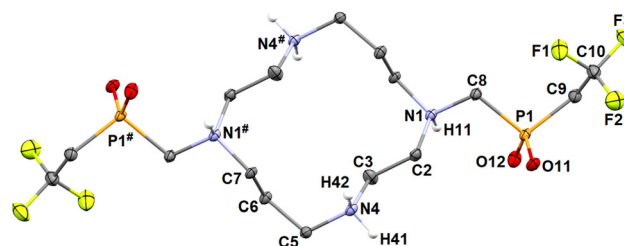


Fig. 3 Molecular structure of one of the independent (H_4L) $^{2+}$ cations found in the crystal structure of (H_4L) $\text{Cl}_2\cdot 4\text{H}_2\text{O}$. Carbon-bound hydrogen atoms are omitted for clarity. Selected centrosymmetry-related atoms are labelled with #.



mation of intramolecular hydrogen bonds, and only a wide network of intermolecular contacts is formed.

Attempts to structurally characterize the ligand in its deprotonated form by the crystallization of H₂L solution neutralised by LiOH to pH *ca.* 9 (a higher pH leads to a slow degradation of the ligand molecule) led to the formation of single crystals of zwitterionic H₂L as a LiCl adduct, H₂L·LiCl·6H₂O. The protonation of the secondary amino groups found in this crystal structure points to their high basicity (see the ESI, Fig. S22†).

Syntheses and solid-state structures of the complexes

Compound H₂3 can also potentially serve as a ligand for transition metal ions. It was tested by the complexation of copper (II) ions. However, the compound H₂3 is insoluble in water, and only slightly soluble in aq. MeOH and EtOH mixtures. Therefore, the complexation reaction was performed in these media. The reaction of H₂3 with Cu(II) affords an emerald green complex somewhat soluble in aq. MeOH, EtOH or *i*-PrOH which can be precipitated by the addition of acetone. Despite a number of attempts, a few single crystals suitable for the determination of the molecular structure of the complex

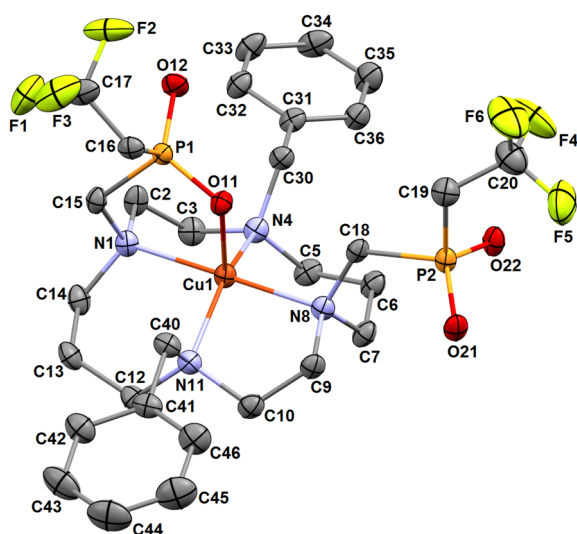


Fig. 4 Molecular structure of *pc*-[Cu(3)] complex found in the crystal structure of *pc*-[Cu(3)]·Cu(AcO)_{1.8}(tfa)_{0.2}·4H₂O·0.5acetone. Hydrogen atoms are omitted for clarity.

were isolated only in the case where a slight excess of copper (II) acetate was used as a metal source and the ligand was used in the form of H₂3·6CF₃CO₂H·2H₂O. The X-ray structural analysis revealed the composition of such crystals to be *pc*-[Cu(3)]·Cu(AcO)_{1.8}(tfa)_{0.2}·4H₂O·0.5acetone with a pentacoordinated (*pc*) geometry of the [Cu(3)] species, leaving one of the phosphinate pendant arms uncoordinated (Fig. 4). Similarly to other *pc*-complexes of cyclam-1,8-bis(methylphosphorus acids) and related *N*-alkylated compounds (1,8-H₄te2p, Fig. 1),³⁹ macrocycles adopt the conformation *trans*-I (according to commonly accepted nomenclature, although the term “*trans*” is misleading in this case as there is no steric possibility to occupy two *trans* positions above and below the plane of the macrocycle).⁵⁴ The coordination sphere of the central Cu(II) ion is intermediate between a trigonal bipyramid (nitrogen atoms N1 and N8 bearing the phosphinate pendant arms placed in apical positions) and a tetragonal pyramid (a N₄ base with an apical oxygen atom), as evidenced by the criterion $\tau = 0.505$.⁵⁵ Excess of Cu(II) and acetate and trifluoroacetate anions present in the solution form a centrosymmetric dimeric core of copper-acetate-like structural motif where the apical positions of the metal coordination spheres are occupied by an oxygen atom of the uncoordinated phosphinate pendant arm from the *pc*-[Cu(3)] species (Fig. S8†). Selected geometric parameters of the coordination sphere are outlined in Tables 1 and S2.† No changes in the UV-Vis spectra upon heating the solution indicate that *pc*-[Cu(3)] species with the conformation *trans*-I cannot be rearranged into other isomers with a different macrocycle conformation. The stability of the conformation *trans*-I is in agreement with previous observations for the complexes of 1,8-H₄te2p ligands alkylated on N4/11 nitrogen atoms (Fig. 1).³⁹

Attempts to prepare complexes of H₂3 with other studied transition metal ions [Co(II), Ni(II) and Zn(II)] by mixing H₂3 with metal chlorides in aq. MeOH solutions and adding ammonia as a base led to the formation of precipitates insoluble in common solvents which cannot be further studied in solution and, therefore, other study of the complexes was impossible. Different behaviours of the Cu(II) complexes and precipitated phases formed with other transition metal ions come probably from the molecular structures – except for the Cu(II) ion, where a pentacoordinated species with the hydrophilic phosphinate arm pointing out of the hydrophobic

Table 1 Coordination distances of metal(II) complexes found in the solid state

Bond (Å)	<i>pc</i> -[Cu(3)]	<i>cis</i> -O,O'-[Co(L)]		<i>cis</i> -O,O'-[Ni(L)]	<i>pc</i> -[Cu(L)]	<i>trans</i> -O,O'-[Cu(L)] ^a	<i>trans</i> -O,O'-[Cu(L)] ^b		<i>cis</i> -O,O'-[Zn(L)]
		Mol. 1	Mol. 2				Mol. 1	Mol. 2	
M–N1	2.102(3)	2.182(2)	2.212(2)	2.154(1)	2.067(1)	2.069(1)	2.068(1)	2.099(1)	2.183(1)
M–N4	2.122(3)	2.115(2)	2.124(2)	2.104(1)	2.017(1)	2.006(1)	2.021(1)	2.024(2)	2.130(1)
M–N8	2.088(3)	2.174(2)	2.189(1)	2.129(1)	2.064(1)	2.069(1) [#]	2.068(1) [#]	2.099(1) [#]	2.217(1)
M–N11	2.119(3)	2.134(2)	2.121(2)	2.083(1)	2.022(1)	2.006(1) [#]	2.021(1) [#]	2.024(2) [#]	2.161(1)
M–O11	2.093(3)	2.094(1)	2.081(1)	2.071(1)	2.148(1)	2.433(1)	2.412(1)	2.372(1)	2.154(1)
M–O21	—	2.085(1)	2.109(1)	2.113(1)	—	2.433(1) [#]	2.412(1) [#]	2.372(1) [#]	2.080(1)

^a *trans*-O,O'-[Cu(L)]·NH₄(Cl_{0.54}Br_{0.46}). ^b *trans*-O,O'-[Cu(L)]·(H₃O)(ClO₄)·H₂O. [#] Centrosymmetry-related atoms (N8 = N1#, N11 = N4#, O21 = O11#).



coordination sphere is formed, other metal ions prefer an octahedral sphere (see below). In these cases, the metal ions are hexadentately wrapped with the $(3)^{2-}$ anion. Hydrophobic benzyl and trifluoroethyl side groups point away and give to the electroneutral complex species a non-polar character. The molecules are thus hydrophobically packed in the solid state and are intact to the solvent.

All studied transition metal ions, Co(II)–Zn(II), were successfully complexed with H₂L. In a typical complexation experiment, an excess of freshly prepared metal(II) hydroxide was reacted with H₂L. After several hours, the excess of M(OH)₂ was filtered off. As Co(OH)₂ could be possibly oxidized, the cobalt(II) complex was prepared by the neutralization of H₂L and CoCl₂ solution with LiOH or by the reaction of aq. solution of H₂L with CoCO₃. The absence of the free ligand in solutions of the complexes was confirmed by the ¹⁹F NMR spectra. In the spectra, one signal was present in the case of the Co(II)–H₂L system but for the other complexes a number of isomeric complex species were obviously initially formed. Heating of the solutions led to spectra with one dominant signal [Ni(II) complex], one broad symmetric signal [Cu(II) complex] and several signals [Zn(II) complex]. The solutions were concentrated and a slow addition of acetone afforded single crystals suitable for structural characterization. For the Co(II), Ni(II) and Zn(II) complexes, crystals contain the *cis*-O,O′-[M(L)] complex species having a somewhat distorted octahedral sphere; particularly, bond angles related to small five-membered chelate rings are somewhat smaller than 90° (Tables 1 and S2†). In all these complexes, the cyclam conformation *cis*-V was found.⁵⁴ All coordinated nitrogen atoms of the macrocycle (N1, N4, N8, N11) have the same stereochemical descriptors according to the Cahn–Ingold–Prelog rules, leading to enantiomeric *R,R,R,R* and *S,S,S,S* pairs. Due to crystallographic centrosymmetry, both enantiomers are present in the crystal structures. However, coordination of the phosphinate pendant arm leads to a new stereocentre on the phosphorus atoms. In the solid state, they have the same absolute configuration as the nitrogen atoms of the macrocycle, resulting in the presence of all-*N*-(*R*)-all-*P*-(*R*) and all-*N*-(*S*)-all-*P*-(*S*) species.

The cobalt(II) complex crystallizes in the form of *cis*-O,O′-[Co(L)]·LiCl·3H₂O. In the crystal structure, two independent complex molecules are present in the independent unit. However, their geometry is very similar and, therefore, only one of them is shown in Fig. 5. Structural overlay of both independent complex molecules is shown in Fig. S9† and selected geometric parameters are listed in Tables 1 and S2.†

In the case of the Ni(II)–H₂L system, single crystals of the composition *cis*-O,O′-[Ni(L)]·3.5H₂O were isolated. This isomer is stable and is not rearranged to the *trans*-O,O′ type even on prolonged reflux in an aq. solution, as evidenced by no changes in the ¹⁹F NMR spectra. Similar preferential formation of the *cis* isomer was previously observed for the Ni(II)–H₄te2p system.⁵⁶ The molecular structure of the *cis*-O,O′-[Ni(L)] complex is very similar to that of the Co(II) complex discussed above (see Tables 1 and S2†) and is shown in Fig. S10.†

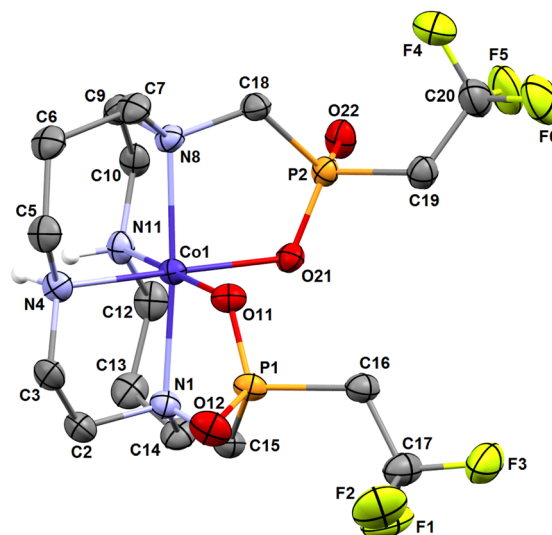


Fig. 5 Molecular structure of *cis*-O,O′-[Co(L)] complex found in the crystal structure of *cis*-O,O′-[Co(L)]·LiCl·3H₂O. Carbon-bound hydrogen atoms are omitted for clarity.

From an isomeric mixture of Zn(II) complexes, crystals suitable for diffraction analysis had the composition *cis*-O,O′-[Zn(L)]·2H₂O·0.5acetone. The geometry of the complex species is very similar to that of the Co(II) and Ni(II) complexes discussed above (Fig. S11, Tables 1 and S2†).

If the complexation of Cu(II) proceeds in a slightly acidic solution (pH 3–4) and at a low temperature, a blue isomer is formed exclusively, which was identified by X-ray diffraction as the pentacoordinated species *pc*-[Cu(L)] with the cyclam conformation *trans*-I.⁵⁴ This blue isomer gradually rearranges to the violet one upon prolonged heating (90 °C, 5 d, Fig. S7†) which was identified as *trans*-O,O′-[Cu(L)] with the cyclam conformation *trans*-III.⁵⁴ If the pH used for the complexation reaction was 7.4, a small amount of the *trans* isomer was formed besides the major *pc*-[Cu(L)] isomer. Both isomers can be separated by TLC/HPLC. From the mixture, the isomers can be isolated by column chromatography on silica using aq. NH₃–EtOH mixture.

The *pc*-isomer is a kinetic product of the complexation reaction and, at room temperature, it rearranges only very slowly into the *trans* one, which is obviously the thermodynamic product; a spot of the *trans*-isomer detectable by TLC appears in a stock solution of the *pc*-isomer after standing at room temperature for several months. The rearrangement can be completed after refluxing an aq. solution of the *pc*-isomer for several days (rearrangement is somewhat faster in neutral than in the acidic solution). This isomerism is fully analogous to the behaviour of Cu(II) complexes of 1,8-H₄te2p (Fig. 1).³⁹

The molecular structures of both isomers are shown in Fig. 6 and 7. Similarly to the *pc*-[Cu(3)] species discussed above and to analogous complexes of the 1,8-H₄te2p ligand family³⁹ and the recently reported *pc*-complex with cyclam derivative bearing two [di(phenyl)phosphoryl]methyl pendant arms,⁵⁷



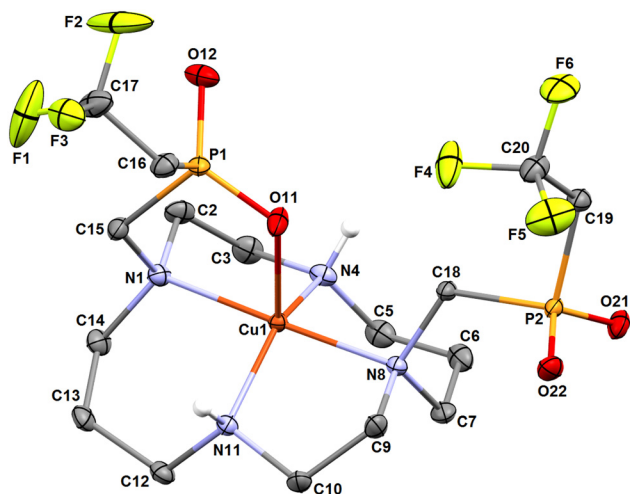


Fig. 6 Molecular structure of *pc*-[Cu(L)] complex found in the crystal structure of *pc*-[Cu(L)]·3H₂O. Carbon-bound hydrogen atoms are omitted for clarity.

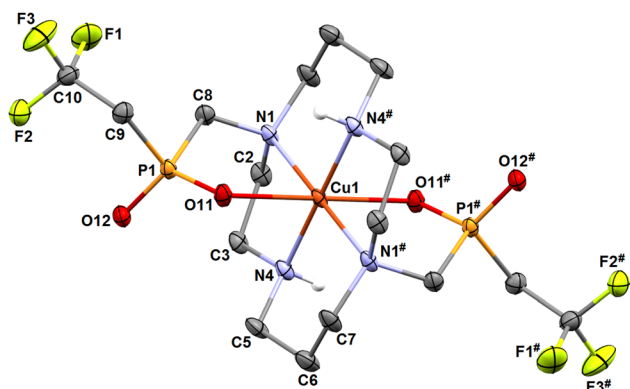


Fig. 7 Molecular structure of *trans*-O,O'-[Cu(L)] complex found in the crystal structure of *trans*-O,O'-[Cu(L)]·NH₄(Cl_{0.54}Br_{0.46}). Carbon-bound hydrogen atoms are omitted for clarity. Selected centrosymmetry-related atoms are labelled with #.

the *pc*-[Cu(L)] species adopts an intermediate structure between a trigonal bipyramid and a square pyramid ($\tau = 0.520$).⁵⁵ The *trans*-O,O'-[Cu(L)] complex is a tetragonal bipyramid with an axial coordination of the pendant arms elongated by the Jahn–Teller phenomenon. Similar elongation was observed in the related structure of *trans*-O,O'-[Cu(1,8-H₂te2p)].³⁹ Selected geometric parameters of the reported structures are outlined in Tables 1 and S2.†

During the preliminary test of kinetic inertness of *trans*-O,O'-[Cu(L)] (see below), single crystals with the composition *trans*-O,O'-[Cu(L)]·(H₃O)(ClO₄)·H₂O were crystallized by cooling of a saturated solution of the complex in boiling 1 M HClO₄. The formation of this phase clearly indicates the extreme kinetic inertness of the complex. In the crystal structure, the oxonium ion serves as a bridge between non-coordinated oxygen atoms of the pendant arms of two neighbouring *trans*-O,O'-[Cu(L)] complex molecules (Fig. S12†). However, geome-

tries of the complex species is essentially the same as those observed in the above discussed crystal structure of *trans*-O,O'-[Cu(L)]·NH₄(Cl_{0.54}Br_{0.46}) (Tables 1 and S2†).

Solution equilibrium studies

The acid–base behaviour of H₂L and stability of its complexes were studied by potentiometric titrations. The calculated constants are listed in Table 2. Similarly to other cyclam-based ligands, H₂L shows two protonation constants in the strongly alkaline region ($\log K_{1,2} > 10$). They correspond to the protonation of the secondary amino groups of the macrocycle and it is consistent with the structure of the ligand's zwitterionic form found in the solid state. In the pH range used for titration (starting from pH 1.6), no further protonation was observed. It points to the low basicity of the amino groups bearing the phosphinate moieties and to the high acidity of the (2,2,2-trifluoroethyl)phosphinic acid pendant arms. It is consistent with the observation that the ligand H₂L crystallizes from aq. acetic acid as the adduct with protonated AcOH (Fig. 2). It should be noted that the compound H₂3 crystallizes from aq. trifluoroacetic acid similarly to the zwitterionic adduct with a protonated trifluoroacetic acid molecule, H₂3·6CF₃CO₂H·2H₂O. To obtain the (H₄L)²⁺ species with a fully protonated macrocycle, crystallization from aq. HCl had to be used (Fig. 3). Consistent with the absence of further protonation in the pH range of potentiometric titration, no change of ¹H, ¹³C, ¹⁹F and ³¹P chemical shifts was observed in the pH range 1–10, and third/more protonation(s) can be suggested to proceed on tertiary amino groups of the macrocycle with $\log K_h < 1$ as can be seen from the chemical shift change in strongly acidic solutions (Fig. S13†). The distribution diagram of the ligand is shown in Fig. S14.† Compared to the related 1,8-phosphin oxide derivative⁵⁷ and the ligands of the H₄te2p phosphonate family,⁵⁸ the ring basicity of H₂L ($\log K_1 + \log K_2$) is lower as a consequence of the electron-withdrawing character of the phosphinate moieties.⁵⁹

Complexation reaction with transition metal ions is relatively slow and, therefore, an out-of-cell method had to be used, with equilibration times of 3 weeks for the Cu(II)–H₂L system and 6 weeks for the other ions. Under these conditions, pentacoordinated isomer *pc*-[Cu(L)] and octahedral *cis*-isomers

Table 2 Stepwise protonation constants ($\log K_n$) of H₂L and its stability constants ($\log \beta_{ML}$) with selected transition metal ions, and comparison with related ligands. Charges of the species are omitted for clarity

Equilibrium	H ₂ L ^b	1,8-H ₄ te2p	Cyclam	H ₄ teta ⁱ
H + L = HL	11.755(3)	— ^{c,d}	11.29 ^g	10.52
H + HL = H ₂ L	10.599(3)	26.41 ^{c,d}	10.19 ^g	10.18
Co + L = <i>cis</i> -[Co(L)]	14.00(8)	19.28 ^e	14.3 ^h	16.38
Ni + L = <i>cis</i> -[Ni(L)]	16.46(8) ^a	21.99 ^e	22.2 ^h	19.83
Cu + L = <i>pc</i> -[Cu(L)]	22.76(5)	25.40 ^f	28.1 ^h	20.49
Zn + L = [Zn(L)]	15.79(3) ^a	20.35 ^e	15.2 ^h	16.40

^a Mixture of isomers (see text). ^b This work. ^c Ref. 58. ^d Overall constant $\log \beta_2$ over two undistinguishable protonation steps. ^e Ref. 40. ^f Ref. 39. ^g Ref. 60. ^h Ref. 37. ⁱ Ref. 38.



of [Co(L)] and [Ni(L)] complexes were formed exclusively, as identified by TLC/HPLC and ^{19}F NMR spectroscopy (see below). However, for the Zn(II)– H_2L system, a mixture of at least three isomers was formed according to the ^{19}F NMR spectra. The same mixture of isomers was obtained in independent reactions (see above). According to the Williams–Irving trend, H_2L shows a very high selectivity for Cu(II) over its neighbours Ni(II) and Zn(II). The selectivity is about 6–7 orders in magnitude, similarly to that found for related 1,8-disubstituted ligands.^{39,40,57} Although the stability constants of the complexes are in general somewhat lower than those reported for the cyclam itself, 1,8- $\text{H}_4\text{te}2\text{p}$ and H_4teta , the stabilities are still sufficient for potential applications as the metal ions are quantitatively complexed under physiological conditions (and the formed complexes are kinetically inert, which is in general more important for possible applications, see below). The Cu(II) ion is fully complexed at pH ~ 3 , whereas full complexations of Ni(II) and Zn(II) proceed at pH ~ 6 , and that of Co(II) ion at pH ~ 7 . The distribution diagrams of the species are shown in Fig. 8.

Solution structure of the complexes

The Co(II), Ni(II) and Zn(II) complexes isolated in the solid state have the *cis-O,O'*-geometry with the cyclam conformation *cis-V*.⁵⁴ In the case of H_2L , all nitrogen atoms have to have formally the same absolute configuration, “all-N-(*R*)” or “all-N-(*S*)”. Coordination of the phosphinate pendant arm results in four different substituents around the phosphorus atom and, thus, *R/S* absolute configurations of the phosphorus atom can be distinguished, leading to diastereoisomerism. In all structurally characterized octahedral complexes of H_2L , the same absolute configuration on both phosphorus atoms and on macrocycle nitrogen atoms was found in the solid state, giving rise to “all-N-(*R*) + P-(*R,R*)” and “all-N-(*S*) + P-(*S,S*)” enanti-

meric pairs. These enantiomers should show only one ^{19}F NMR signal due to effective C_2 -symmetry.

Overlaid ^{19}F NMR spectra are shown in Fig. 9 for visual comparison (induced shift, linewidth) of the measured ^{19}F NMR signals of the studied complexes.

The ^{19}F NMR spectra of the equilibrated solution of the Co(II)– H_2L complex show one broad symmetric signal at -38.6 ppm (Fig. S1†) which agrees with a presence of the *cis-O,O'*-species found in the solid state. In contrast, in a solution of the Ni(II) complex, three signals were found – a major signal at -47.1 ppm ($\sim 80\%$) and two equal minor signals at -43.7 and -47.7 ppm (each $\sim 10\%$), as shown in Fig. S2.† The *pc*-[Cu(L)] isomer shows two very broad signals in the ^{19}F NMR spectra as expected for the coordinated and the non-coordinated pendant arms (-52.6 ppm and -53.2 ppm, Fig. S5†), whereas the *trans-O,O'*-[Cu(L)] isomer shows one symmetric signal (-52.7 ppm, Fig. S6†). In the case of the *pc*-[Cu(L)] isomer, no coalescence of both signals was observed upon heating. It points that the pentacoordinated sphere is not fluxional. In a solution of the Zn(II) complex, pseudo-quartets (due to F–P,H couplings) centred at -57.15 ppm ($\sim 40\%$), -57.23 ppm ($\sim 55\%$) and -57.30 ppm ($\sim 5\%$) were observed (Fig. S3†). An analogous pattern was found also in the ^{31}P NMR spectra (30.1 ppm, $\sim 55\%$; 29.4 ppm, $\sim 5\%$; 28.7 ppm, $\sim 40\%$, Fig. S4†). The ^{31}P NMR spectra of other complexes do not show any measurable signals due to the strong paramagnetic effect on the phosphorus atoms.

Based on the numbers of the signals in the ^{19}F NMR spectra, one can conclude that a mixture of isomers is present in the solutions of the Ni(II) and Zn(II) complexes. The assignment of the signals was performed by the measurement of the ^{19}F NMR spectra of freshly dissolved solid samples: batches of crystalline material were prepared from which unit cell parameters were determined for several selected crystals to confirm that they correspond to *cis-O,O'*-[Ni(L)]·3.5 H_2O and *cis-O,O'*-[Zn

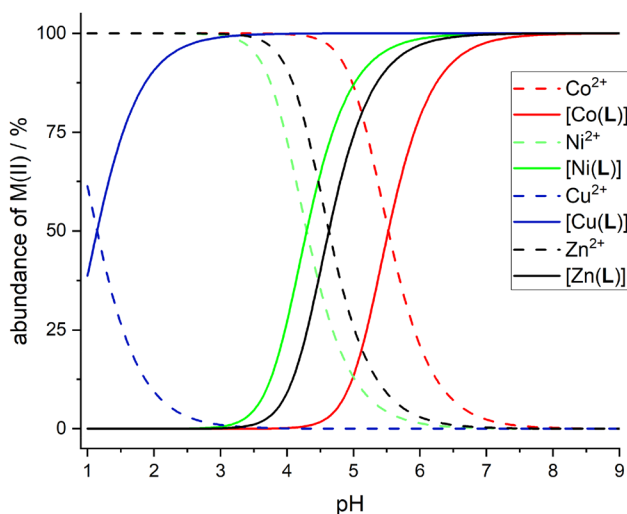


Fig. 8 Distribution diagrams of the $\text{M}(\text{II})$ – H_2L systems; $c(\text{M}) = c(\text{H}_2\text{L}) = 0.004$ M. Co(II) – red lines, Ni(II) – green lines, Cu(II) – blue lines, Zn(II) – black lines. Full lines show distribution of the $[\text{M}(\text{L})]$ complex species, dashed lines show distribution of the free metal aqua ions.

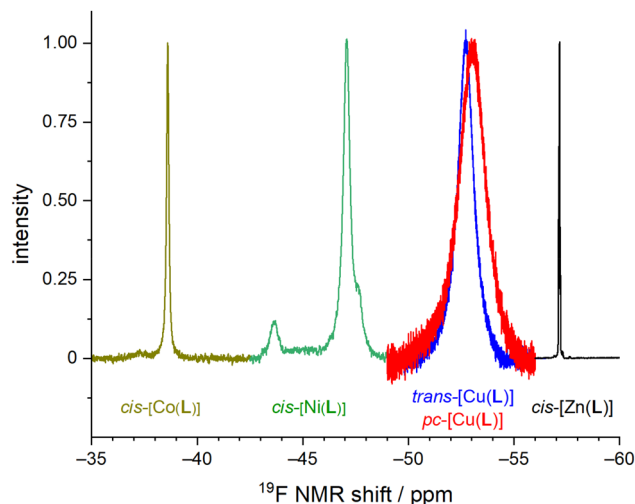


Fig. 9 Representation of normalized ^{19}F NMR spectra of studied $\text{M}(\text{II})$ – H_2L complexes.



(L)]·2H₂O·0.5(C₃H₆O), respectively. In the case of the Ni(II) complex, the ¹⁹F NMR spectra contains all three signals as described above immediately after dissolution. Thus, an equilibration is evidently very fast process (<3 min). As two minor signals have the same intensity, the pair of minor signals probably corresponds to “all-N-(R) + P-(R,S)” and “all-N-(S) + P-(S,R)” enantiomers formed by a mutual exchange of the coordinated and non-coordinated oxygen atoms of one pendant arm. It seems more accessible than a rearrangement of macrocycle conformation to *e.g.* conformation *trans*-III as Ni(II) complexes of cyclam-based ligands are rigid and such a rearrangement is usually energetically demanding and a very slow process.⁵⁶ In the case of the Zn(II) complex, the situation is much more complicated. Freshly dissolved sample of *cis*-O,O′-[Zn(L)] with “all-N-(R) + P-(R,R)” and “all-N-(S) + P-(S,S)” configurations shows a multiplet centred at δF = −57.15 ppm (pseudo-quartet due to F–H,P coupling) and δP = 28.69 ppm (quartet due to P–F coupling in ³¹P{¹H} spectra), so these signals can be assigned to the isomer found in the solid state. However, the other two signals increase gradually, and one of them becomes finally dominant. The final equilibrated mixture (5 d, 80 °C) shows the same spectra containing three multiplets as described above for the synthetic mixture and the signal of the original “all-N-(R) + P-(R,R)” and “all-N-(S) + P-(S,S)” enantiomers has finally only 40% abundance.

Obviously, at least two new isomeric complex species are present in the solution. They could be *e.g.* diastereoisomers “all-N-(R) + P-(R,S)” and “all-N-(R) + P-(S,S)” and their enantiomers as the phosphinate group oxygen atom exchange seems to be the most accessible process. However, some signal overlap has to be supposed as such a mixture should show four individual signals. Alternatively, a partial change of the macrocycle conformation *cis*-V to other possible conformations could occur; such a process has been documented well for Zn(II) complexes of cyclam derivatives.⁶¹

Kinetic inertness of the complexes

Kinetic inertness is suggested as a more important parameter for *in vivo* use than thermodynamic stability^{25,62} and, therefore, it was roughly determined by acid-assisted dissociation in 1 M HCl. *pc*-[Cu(L)] was found to be moderately inert with a

half-life of 15.4 min at room temperature. However, the *trans*-O,O′-[Cu(L)] complex was found to be extremely inert; no change in the UV-Vis spectra was found at room temperature after 24 h. Therefore, dissociation reaction was followed at 90 °C. Under these conditions, dissociation half-time of 2.8 h was observed (Fig. S15†). The behaviour of both Cu(II)–H₂L complexes is very similar to that of Cu(II) complexes of 1,8-H4te2p (Fig. 1).³⁹

As the complexes of Co(II) and Ni(II) ions show no significant absorption in the near UV region and d–d transition bands have a very low intensity, their kinetic inertness was followed by ¹⁹F NMR. Both *cis*-O,O′-[M(L)] were found to be very inert. The observed half-life of *cis*-O,O′-[Co(L)] in 1 M HCl at 25 °C was 3.0 h (Fig. S16†). In the case of *cis*-O,O′-[Ni(L)], no changes in the ¹⁹F NMR spectra were found after standing for 24 h under these conditions and, therefore, temperature was increased to 90 °C. At such an increased temperature, the dissociation half-life time was 36 min (Fig. S16†). The inertness of *cis*-O,O′-[Ni(L)] is thus comparable or somewhat lower than that reported for the *trans*-O,O′-[Ni(1,8-tfe₂cyclam-R₂)] family, but significantly higher compared to that of the *cis*-isomer of Ni(II) complex with 1,8-tfe₂cyclam with no coordinating pendant arms (Fig. 1, R = H).³²

¹⁹F NMR relaxation of the complexes

As the distance between the metal centre and the fluorine atoms is a crucial parameter influencing the relaxation rate of the ¹⁹F NMR signal, it is compiled in Table 3. It can be seen that the geometry of the coordination sphere influences the M...F distance only negligibly – in the *cis*-isomers, the distances are in the range of 5.6–6.5 Å, which is very similar to range of 5.8–6.8 Å found in the *pc*-Cu(II) complexes for the coordinated pendant arm and 5.8–7.0 Å found for the *trans*-Cu(II) species. The range of the distances of fluorine atoms belonging to the non-coordinated pendant arms in the *pc*-Cu(II) complexes is slightly larger, 7.2–7.7 Å and 5.1–7.0 Å in the *pc*-[Cu(3)] and *pc*-[Cu(L)] complexes, respectively. The observed distances are relevant for their significant influence on the relaxation times.³⁰ As the trifluoroethyl group undergoes free rotation, mean distances (Table 3) are used in the following discussion, although effective distances in the solution can

Table 3 Distances between fluorine atoms and the central metal ions found in the crystal structures of studied complexes

Distances (Å)	<i>pc</i> -[Cu(3)] ^a	<i>cis</i> -O,O′-[Co(L)]			<i>cis</i> -O,O′-[Ni(L)]	<i>pc</i> -[Cu(L)] ^a	<i>trans</i> -O,O′-[Cu(L)] ^b	<i>trans</i> -O,O′-[Cu(L)] ^f		<i>cis</i> -O,O′-[Zn(L)]
		Mol. 1	Mol. 2	Mol. 1				Mol. 2		
M...F1	5.884(3)	5.570(1)	5.702(1)	5.620(1)	5.813(1)	5.813(1)	5.809(1)	5.904(1)	5.637(1)	
M...F2	6.284(3)	6.266(1)	6.205(1)	6.240(1)	6.338(1)	6.414(1)	6.370(1)	6.377(1)	6.362(1)	
M...F3	6.768(3)	6.484(2)	6.413(1)	6.415(1)	6.701(1)	6.908(1)	6.973(1)	6.993(1)	6.502(1)	
M...F4	7.170(3)	5.815(2)	5.868(2)	5.596(1)	5.075(1)	5.813(1) [#]	5.809(1) [#]	5.904(1) [#]	5.668(1)	
M...F5	7.647(3)	6.330(1)	6.322(1)	6.319(1)	6.590(1)	6.414(1) [#]	6.370(1) [#]	6.377(1) [#]	6.261(1)	
M...F6	7.747(3)	6.634(1)	6.658(1)	6.478(1)	6.966(1)	6.908(1) [#]	6.973(1) [#]	6.993(1) [#]	6.439(1)	
Average	6.31/7.52 ^s	6.18	6.19	6.11	6.28/6.21 ^s	6.38	6.38	6.42	6.14	

^a F1–F3 belong to the coordinated pendant arm, F4–F6 belong to the non-coordinated pendant arm. ^b *trans*-O,O′-[Cu(L)]·NH₄(Cl_{0.54}Br_{0.46}). ^c *trans*-O,O′-[Cu(L)]·(H₃O)(ClO₄)·H₂O. [#] Centrosymmetry-related atoms (F4 = F1#, F5 = F2#, F6 = F3#). ^s Fluorine atoms of coordinated/non-coordinated pendant arms.



differ due to molecular flexibility and can be shorter.³⁰ Solutions of the prepared complexes underwent detailed ¹⁹F NMR study. The T_1 and T_2^* relaxation times were measured at available magnetic fields (7.05/9.40/14.1 T, 282/376/565 MHz) at 25 and 37 °C and the results are outlined in Table 4. The measurements confirmed significant shortening of the relaxation times in all studied paramagnetic complexes. A source of the T_1 shortening lies in the dipolar mechanism as the number of bonds between the metal ion and fluorine atom is too high (5) to consider a significant contact contribution and Curie relaxation can be neglected for small molecules with small magnetic moments.^{30,34}

The *cis-O,O'*-[Co(L)] species showed longitudinal relaxation times in the range 30–40 ms which is very convenient for practical utilization. It is *ca.* 2–3 times longer (at the same magnetic fields and temperatures) compared to that of Co(II) complexes of 1,8-tfe₂-cyclams (Fig. 1, R = CH₂CO₂H, CH₂PO₃H₂) studied previously.³⁴ The difference comes from longer distances between the central metal ion and fluorine atoms in *cis-O,O'*-[Co(L)] when compared to that in the complexes of 1,8-tfe₂-cyclams (6.19 Å and 5 bonds for *cis-O,O'*-[Co(L)] compared to 5.25 Å and 4 bonds for Co(II)-1,8-tfe₂-cyclams). Furthermore, the ¹⁹F NMR signal is relatively narrow (half-width 40–90 Hz depending on the temperature and magnetic field used) when compared to other studied paramagnetic complexes {Ni(II) 100–170 Hz, *pc*-[Cu(L)] 370–640 Hz, *trans-O,O'*-[Cu(L)] 200–450 Hz}, although in combination with a relatively long T_1 it gives a rather low T_2^*/T_1 ratio (0.1–0.2).

The ¹⁹F NMR signal of *cis-O,O'*-[Ni(L)] relaxes significantly faster than that of the Co(II) complex but it shows *ca.* 2-times slower relaxation ($T_1 \sim 3$ –4 ms) in comparison with that of the Ni(II) complexes of 1,8-tfe₂-cyclam derivatives (Fig. 1, R = H, CH₂CO₂H, CH₂PO₃H₂, (CH₂)₂NH₂, pyrid-2-ylmethyl), whose T_1 was typically in range of 1–2 ms.^{31,32} It corresponds to the distance change (average M...F 6.11 Å for the *cis-O,O'*-[Ni(L)] complex compared to 5.16–5.34 for the Ni(II)-1,8-tfe₂-cyclam complexes). The relaxation time is still too short for a comfortable standard imaging, but the high T_2^*/T_1 ratio 0.6–0.8 of the signal can be potentially utilized in special imaging experiments.^{63,64} For the agent useful in standard imaging, a longer separation of the metal ion and fluorine atoms is obviously needed when using Ni(II) ion, as evidenced by T_1 in the order of tens of milliseconds observed for Ni(II) complexes of cross-bridged cyclam containing [(trifluoromethyl)phenyl]acetamide pendant arms (Fig. 1, 8 bond separation, 7.28 Å, 10 ms; 9 bond separation, 8.72 Å, 29 ms).³³

Observed T_1 for the Cu(II)-H₂L complexes (*ca.* 5–9 ms) is slightly lower than values found for isomeric Cu(II) complexes of 1,8-(tfe-NHCH₂CH₂)₂cyclam (7–12 ms)⁴² whereas the average M...F distances found in the Cu(II)-H₂L complexes are somewhat longer (6.36 Å) than those observed for the Cu(II)-1,8-(tfe-NHCH₂CH₂)₂cyclam (5.6–6.1 Å).⁴² However, the signals of the Cu(II)-H₂L complexes are very broad. The T_2^*/T_1 ratio is *ca.* 0.1 for the pentacoordinated and *ca.* 0.2 for the *trans-O,O'*-[Cu(L)] isomer, respectively.

The T_1 data acquired at 25 °C have been further assessed using the equation set of the Bloch–Redfield–Wangsness

Table 4 Selected relaxometric characteristics of ¹⁹F NMR signal of studied compounds (buffer, 25/37 °C). The T_2 times were measured with CPMG sequence [free ligand and Zn(II)-complex] or calculated from half-widths of the paramagnetic signals (T_2^* for other complexes). Chemical shifts are corrected for bulk magnetic susceptibility effect

Parameter	H ₂ L	<i>cis-O,O'</i> -[Co(L)]	<i>cis-O,O'</i> -[Ni(L)]	<i>pc</i> -[Cu(L)]	<i>trans-O,O'</i> -[Cu(L)]	<i>cis-O,O'</i> -[Zn(L)] ^d
pH	7.4	8.0 ^a	7.4	4.0 ^b	7.4	7.4
¹⁹ F δ/ppm	-57.13	-38.6	-47.1	-52.9 ^c	-52.7	-57.15
$T_1^{25\text{ °C}}$ (282 MHz)/ms	1.38(7) × 10 ³	35(2)	3.6(2)	6.5(3)	5.1(3)	1.11(6) × 10 ³
$T_2^{25\text{ °C}}$ (282 MHz)/ms	—	7.2(7)	2.9(3)	0.5(1)	0.7(1)	—
$(T_2/T_1)^{282\text{ MHz}, 25\text{ °C}}$	—	0.21	0.81	0.08	0.14	—
$T_1^{37\text{ °C}}$ (282 MHz)/ms	1.79(9) × 10 ³	41(2)	4.5(3)	8.5(4)	7.0(4)	1.42(7) × 10 ³
$T_2^{37\text{ °C}}$ (282 MHz)/ms	—	3.5(3)	3.1(3)	0.7(1)	0.8(1)	—
$(T_2/T_1)^{282\text{ MHz}, 37\text{ °C}}$	—	0.09	0.69	0.08	0.11	—
$T_1^{25\text{ °C}}$ (376 MHz)/ms	1.11(5) × 10 ³	33(2)	3.3(2)	5.9(3)	5.4(3)	0.87(4) × 10 ³
$T_2^{25\text{ °C}}$ (376 MHz)/ms	0.90(5) × 10 ³	6.3(6)	2.2(2)	0.5(1)	0.9(1)	0.61(6) × 10 ³
$(T_2/T_1)^{376\text{ MHz}, 25\text{ °C}}$	0.81	0.19	0.67	0.08	0.17	0.70
$T_1^{37\text{ °C}}$ (376 MHz)/ms	1.29(6) × 10 ³	35(2)	3.6(2)	8.7(4)	6.7(3)	1.04(5) × 10 ³
$T_2^{37\text{ °C}}$ (376 MHz)/ms	0.92(5) × 10 ³	4.7(5)	2.5(2)	0.6(1)	1.1(1)	0.87(4) × 10 ³
$(T_2/T_1)^{376\text{ MHz}, 37\text{ °C}}$	0.71	0.13	0.69	0.07	0.16	0.84
$T_1^{25\text{ °C}}$ (565 MHz)/ms	0.74(4) × 10 ³	28(2)	3.2(2)	7.5(4)	6.1(3)	0.60(3) × 10 ³
$T_2^{25\text{ °C}}$ (565 MHz)/ms	0.60(3) × 10 ³	6.3(6)	1.9(2)	0.6(1)/0.8(1) ^c	1.2(1)	0.48(3) × 10 ³
$(T_2/T_1)^{565\text{ MHz}, 25\text{ °C}}$	0.81	0.23	0.59	0.10	0.20	0.80
$T_1^{37\text{ °C}}$ (565 MHz)/ms	0.94(5) × 10 ³	33(2)	3.9(2)	9.3(5)	7.2(4)	0.77(4) × 10 ³
$T_2^{37\text{ °C}}$ (565 MHz)/ms	0.74(4) × 10 ³	3.4(3)	2.4(2)	0.7(1)/1.0(1) ^c	1.5(1)	0.62(3) × 10 ³
$(T_2/T_1)^{565\text{ MHz}, 37\text{ °C}}$	0.79	0.10	0.62	0.09	0.21	0.81

^a The pH 8.0 was used to assure the full complexation. ^b The pH 4.0 was used to avoid formation of the *trans-O,O'*-isomer. ^c The pendant arms are not equivalent in the *pc*-[Cu(L)] complex – one is coordinated, whereas the second is not. However, deconvolution of the measured signal into two peaks –52.6 and –53.2 ppm was possible only at 14.1 T. Both signals are very broad and strongly overlap (Fig. S5†). At lower fields, nearly symmetric signal was observed (Fig. 9). ^d Mixture of isomers is present in solution; the data are given for the isomer characterized by X-ray crystallography.



theory.³⁰ Preliminary calculation confirmed that the contribution of Curie relaxation is for the presented set of complexes negligible and, thus, only the dipolar relaxation mechanism was considered. This phenomenon is quantified by eqn (1):

$$R_1^{\text{DD}} = \frac{2}{15} \left(\frac{\mu_0}{4\pi} \right)^2 \gamma_F^2 \mu_{\text{eff}}^2 \beta_M^2 \left(\frac{7\tau_c}{1 + \omega_e^2 \tau_c^2} + \frac{3\tau_c}{1 + \omega_F^2 \tau_c^2} \right) \quad (1)$$

where R_1^{DD} is the dipole–dipole relaxation rate, μ_0 is vacuum permeability, π is Ludolph's number, γ_F is the magnetogyric ratio of the fluorine nucleus, μ_{eff} is the effective magnetic moment of the paramagnetic metal ion, β_M is the Bohr magneton, d_{MF} is the average effective distance between the metal ion and the fluorine atom, ω_e and ω_F are the Larmor frequencies of the electron and fluorine nuclei, respectively, and τ_c is the total correlation time, given for the dipolar interaction by eqn (2):

$$\tau_c^{-1} = \tau_e^{-1} + \tau_R^{-1} \quad (2)$$

where τ_e is the electronic relaxation time and τ_R is the rotational correlation time. The parameters relevant for the given system are thus τ_R , τ_e , d_{MF} and μ_{eff} . Of those, the highest uncertainty is brought by τ_e , which – for a particular metal ion – can reach different values covering a few orders in magnitude. However, as the number of the data is relatively small (although τ_R and d_{MF} can be considered the same for at least isostructural complexes), full fitting of the data is not reliable. Therefore, we fixed τ_R to 170 ps, the value estimated using the Debye–Stokes–Einstein equation. Magnetic moments were set to the mean literature values³⁰ to obtain a close comparison of the results with the reported data (in general, the used values of μ_{eff} are somewhat higher than those predicted by the spin-only formula). The distances d_{MF} were fixed to the values obtained from the crystal structures (Table 3; except the value

for *trans*-*O,O'*-[Cu(L)], which needed to be slightly shortened to obtain good fit of the data), and the last parameter – τ_e – was calculated. The resulting fits are shown in Fig. 10. The values of τ_e fall in the expected range and are in good agreement with the literature data.³⁰

Of the used paramagnetic metal ions, the situation is the most straightforward for the Co^{2+} complex, as τ_e of this ion is significantly shorter than τ_R (by *ca.* 2 orders of magnitude) and, thus, τ_c is governed dominantly by τ_e . In contrast, for Ni^{2+} and Cu^{2+} , contributions of both τ_e and τ_R to τ_c are significant, and thus, their values significantly correlate (*i.e.* a slight change in the suggested τ_R brings a significant change in τ_e , and *vice versa*).

Conclusions

A new cyclam-based ligand substituted in the 1,8-positions with two (2,2,2-trifluoroethyl)phosphinate pendant arms was found to bind divalent transition metal ions $\text{Co}(\text{II})$, $\text{Ni}(\text{II})$, $\text{Cu}(\text{II})$ and $\text{Zn}(\text{II})$ in stable complexes with a high selectivity for the $\text{Cu}(\text{II})$ ion. The $\text{Cu}(\text{II})$ ion forms two isomeric complexes: the pentacoordinated isomer *pc*-[Cu(L)] is formed as the kinetic product of the complexation reaction and rearranges to the thermodynamic product, the octahedral *trans*-*O,O'*-[Cu(L)] isomer. The $\text{Co}(\text{II})$, $\text{Ni}(\text{II})$ and $\text{Zn}(\text{II})$ ions form octahedral *cis*-*O,O'*-[M(L)] complexes. The complexes are kinetically inert with respect to acid-assisted dissociation. Paramagnetic metal ion complexes show very short relaxation times of the ^{19}F NMR signal {*cis*-*O,O'*-[Co(L)] 30–40 ms, *cis*-*O,O'*-[Ni(L)] 3–4 ms, *pc*-[Cu(L)] ~9 ms, *trans*-*O,O'*-[Cu(L)] ~7 ms; 37 °C, 7–14 T}, which is a result of a short distance between the paramagnetic metal ion and the fluorine atoms (mean values found in the crystal structures are ~6.1–6.4 Å). It makes these systems promising and potentially useful as contrast agents in ^{19}F magnetic resonance imaging (^{19}F MRI).

Author contributions

FK: investigation, formal analysis, and writing. JK: conceptualization, investigation, formal analysis, supervision, and writing. IC: investigation and formal analysis. JH: investigation. VK: formal analysis. PH: conceptualization, funding acquisition, supervision, and writing.

Conflicts of interest

There are no conflicts to declare.

Acknowledgements

Financial support of the Czech Science Foundation (GAČR) 22-34083S is acknowledged. The project was performed in the frame of COST-action CA 18202 NECTAR.

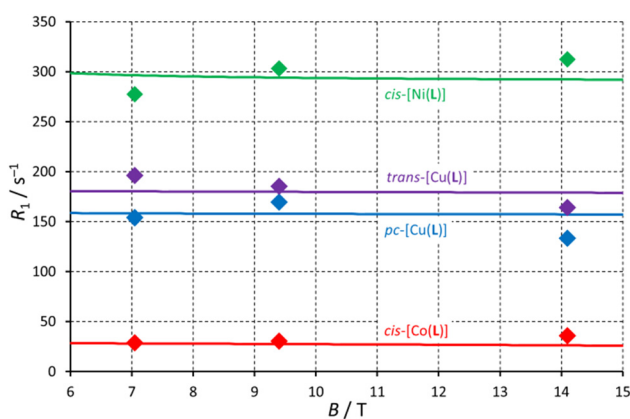


Fig. 10 Longitudinal relaxation rates of studied paramagnetic complexes. Parameters used for the fitting: $\tau_R = 170$ ps (common for all complexes), $d_{\text{MF}} = 6.18$ Å and $\mu_{\text{eff}} = 4.7$ for *cis*-*O,O'*-[Co(L)], $d_{\text{MF}} = 6.11$ Å and $\mu_{\text{eff}} = 3.5$ for *cis*-*O,O'*-[Ni(L)], $d_{\text{MF}} = 6.25$ Å and $\mu_{\text{eff}} = 1.9$ for *pc*-[Cu(L)] and $d_{\text{MF}} = 6.30$ Å and $\mu_{\text{eff}} = 1.9$ for *trans*-*O,O'*-[Cu(L)]. Calculated values of τ_e were 1.0×10^{-12} s (*cis*-*O,O'*-[Co(L)]), 8.5×10^{-11} s (*cis*-*O,O'*-[Ni(L)]), 4×10^{-10} s (*pc*-[Cu(L)]) and 5×10^{-10} s (*trans*-*O,O'*-[Cu(L)]), respectively.



References

- 1 *The Chemistry of Contrast Agents in Medical Magnetic Resonance Imaging*, ed. A. E. Merbach, L. Helm and É. Tóth, John Wiley & Sons, 2nd ed., 2013.
- 2 C. S. Bonnet and É. Tóth, *Chimia*, 2016, **70**, 102–108.
- 3 B. Condon, *EMPA J.*, 2011, **2**, 403–410.
- 4 Y. A. Pirogov, *Phys. Procedia*, 2016, **82**, 3–7.
- 5 D. Bartusik-Aebisher, Z. Bober, J. Zalejska-Fiolka, A. Kawczyk-Krupka and D. Aebisher, *Molecules*, 2022, **27**, 6493.
- 6 E. T. Ahrens, R. Flores, H. Xu and P. A. Morel, *Nat. Biotechnol.*, 2005, **23**, 983–987.
- 7 Y. Mo, C. Huang, C. Liu, Z. Duan, J. Liu and D. Wu, *Macromol. Rapid Commun.*, 2023, 2200744.
- 8 B. L. Bona, O. Koshkina, C. Chirizzi, V. Dichiarante, P. Metrangolo and F. Baldelli Bombelli, *Acc. Mater. Res.*, 2023, **4**, 71–85.
- 9 K. Waxman, *Ann. Emerg. Med.*, 1986, **15**, 1423–1424.
- 10 K. C. Lowe, *Blood Rev.*, 1999, **13**, 171–184.
- 11 L. Mignon, J. Magat, O. Schakman, E. Marbaix, B. Gallez and B. F. Jordan, *Magn. Reson. Med.*, 2013, **69**, 248–254.
- 12 E. Maevsky, G. Ivanitsky, L. Bogdanova, O. Axenova, N. Karmen, E. Zhiburt, R. Senina, S. Pushkin, I. Maslennikov, A. Orlov and I. Marinicheva, *Artif. Cells, Blood Substitutes, Biotechnol.*, 2005, **33**, 37–46.
- 13 R. P. Mason, P. P. Antich, E. E. Babcock, J. L. Gerberich and R. L. Nunnally, *Magn. Reson. Imaging*, 1989, **7**, 475–485.
- 14 B. J. Dardzinski and C. H. Sotak, *Magn. Reson. Med.*, 1994, **32**, 88–97.
- 15 G. M. Lanza, X. Yu, P. M. Winter, D. R. Abendschein, K. K. Karukstis, M. J. Scott, L. K. Chinen, R. W. Fuhrhop, D. E. Scherrer and S. A. Wickline, *Circulation*, 2002, **106**, 2842–2847.
- 16 A. M. Morawski, P. M. Winter, X. Yu, R. W. Fuhrhop, M. J. Scott, F. Hockett, J. D. Robertson, P. J. Gaffney, G. M. Lanza and S. A. Wickline, *Magn. Reson. Med.*, 2004, **52**, 1255–1262.
- 17 S. D. Caruthers, A. M. Neubauer, F. D. Hockett, R. Lamerichs, P. M. Winter, M. J. Scott, P. J. Gaffney, S. A. Wickline and G. M. Lanza, *Invest. Radiol.*, 2006, **41**, 305–312.
- 18 A. M. Neubauer, J. Myerson, D. Caruthers, F. D. Hockett, P. M. Winter, J. Chen, P. J. Gaffney, J. D. Robertson, G. M. Lanza and S. A. Wickline, *Magn. Reson. Med.*, 2008, **60**, 1066–1072.
- 19 Y. Li, J. Cui, C. Li, H. Zhou, J. Chang, O. Aras and F. An, *ChemMedChem*, 2022, **17**, e202100701.
- 20 P. Hermann, J. Blahut, J. Kotek and V. Herynek, *Met. Ions Life Sci.*, 2021, **22**, 239–270.
- 21 D. Janasik and T. Krawczyk, *Chem. – Eur. J.*, 2022, **28**, e202102556.
- 22 A. Li, X. Luo, D. Chen, L. Li, H. Lin and J. Gao, *Anal. Chem.*, 2023, **95**, 70–82.
- 23 A. M. Kenwright, I. Kuprov, E. De Luca, D. Parker, S. U. Pandya, P. K. Senanayake and D. G. Smith, *Chem. Commun.*, 2008, 2514–2516.
- 24 R. Pujales-Paradela, T. Savić, P. Pérez-Lourido, D. Esteban-Gómez, G. Angelovski, M. Botta and C. Platas-Iglesias, *Inorg. Chem.*, 2019, **58**, 7571–7583.
- 25 E. Brücher, G. Tircsó, Z. Baranyai, Z. Kovács and A. D. Sherry, in *The Chemistry of Contrast Agents in Medical Magnetic Resonance Imaging*, ed. A. E. Merbach, L. Helm and É. Tóth, John Wiley & Sons, 2nd ed., 2013, ch. 4.
- 26 J. Neburkova, A. M. Rulseh, S. L. Y. Chang, H. Raabova, J. Vejpravova, M. Dracinsky, J. Tarabek, J. Kotek, M. Pingle, P. Majer, J. Vymazal and P. Cigler, *Nanoscale Adv.*, 2020, **2**, 5567–5571.
- 27 K. Srivastava, E. A. Weitz, K. L. Peterson, M. Marjańska and V. C. Pierre, *Inorg. Chem.*, 2017, **56**, 1546–1557.
- 28 M. Yu, B. S. Bouley, D. Xie and E. L. Que, *Dalton Trans.*, 2019, **48**, 9337–9341.
- 29 A. Gupta, P. Caravan, W. S. Price, C. Platas-Iglesias and E. M. Gale, *Inorg. Chem.*, 2020, **59**, 6648–6678.
- 30 M. Zalewski, D. Janasik, A. Wierzbička and T. Krawczyk, *Inorg. Chem.*, 2022, **61**, 19524–19542.
- 31 J. Blahut, P. Hermann, A. Gálisová, V. Herynek, I. Císařová, Z. Tošner and J. Kotek, *Dalton Trans.*, 2016, **45**, 474–478.
- 32 J. Blahut, K. Bernásek, A. Gálisová, V. Herynek, I. Císařová, J. Kotek, J. Lang, S. Matějková and P. Hermann, *Inorg. Chem.*, 2017, **56**, 13337–13348.
- 33 R. Pujales-Paradela, T. Savić, I. Brandariz, P. Pérez-Lourido, G. Angelovski, D. Esteban-Gómez and C. Platas-Iglesias, *Chem. Commun.*, 2019, **55**, 4115–4118.
- 34 J. Blahut, L. Benda, J. Kotek, G. Pintacuda and P. Hermann, *Inorg. Chem.*, 2020, **59**, 10071–10082.
- 35 D. Xie, M. Yu, R. T. Kadakia and E. L. Que, *Acc. Chem. Res.*, 2020, **53**, 2–10.
- 36 J. S. Enriquez, M. Yu, B. S. Bouley, D. Xie and E. L. Que, *Dalton Trans.*, 2018, **47**, 15024–15030.
- 37 *NIST Standard Reference Database 46 (Critically Selected Stability Constants of Metal Complexes), Version 7.0*, 2003, distributed by NIST standard Reference Data, Gaithersburg, MD 20899, USA.
- 38 S. Chaves, R. Delgado and J. J. R. F. da Silva, *Talanta*, 1992, **39**, 249–254.
- 39 J. Kotek, P. Lubal, P. Hermann, I. Císařová, I. Lukeš, T. Godula, I. Svobodová, P. Táborský and J. Havel, *Chem. – Eur. J.*, 2003, **9**, 233–248.
- 40 I. Svobodová, P. Lubal, J. Plutnar, J. Havlíčková, J. Kotek, P. Hermann and I. Lukeš, *Dalton Trans.*, 2006, 5184–5197.
- 41 J. Havlíčková, H. Medová, T. Vítha, J. Kotek, I. Císařová and P. Hermann, *Dalton Trans.*, 2008, 5378–5386.
- 42 Z. Kotková, F. Koucký, J. Kotek, I. Císařová, D. Parker and P. Hermann, *Dalton Trans.*, 2023, **52**, 1861–1875.
- 43 V. Herynek, M. Martinisková, Y. Bobrova, A. Gálisová, J. Kotek, P. Hermann, F. Koucký, D. Jiráček and M. Hájek, *Magn. Reson. Mater. Phys., Biol. Med.*, 2019, **32**, 115–122.
- 44 W. L. F. Armarego and C. L. L. Chai, *Purification of Laboratory Chemicals*, Butterworth Heinemann An imprint of Elsevier Science, 5th edn, 2003.



- 45 G. Royal, V. Dahaoui-Gindrey, S. Dahaoui, A. Tabard, R. Guillard, P. Pullumbi and C. Lecomte, *Eur. J. Org. Chem.*, 1998, 1971–1975.
- 46 L. Krause, R. Herbst-Irmer, G. M. Sheldrick and D. Stalke, *J. Appl. Crystallogr.*, 2015, **48**, 3–10.
- 47 (a) G. M. Sheldrick, *SHELXT2014/5. Program for Crystal Structure Solution from Diffraction Data*, University of Göttingen, Göttingen, 2014; (b) G. M. Sheldrick, *Acta Crystallogr., Sect. A: Found. Crystallogr.*, 2008, **64**, 112–122.
- 48 (a) C. B. Hübschle, G. M. Sheldrick and B. Dittrich, *ShelXle: a Qt graphical user interface for SHELXL*, University of Göttingen, Göttingen, 2014; (b) C. B. Hübschle, G. M. Sheldrick and B. Dittrich, *J. Appl. Crystallogr.*, 2011, **44**, 1281–1284; (c) G. M. Sheldrick, *SHELXL-2014/7. Program for Crystal Structure Refinement from Diffraction Data*, University of Göttingen, Göttingen, 2014; (d) G. M. Sheldrick, *Acta Crystallogr., Sect. C: Struct. Chem.*, 2015, **71**, 3–8.
- 49 M. Försterová, I. Svobodová, P. Lubal, P. Táborský, J. Kotek, P. Hermann and I. Lukeš, *Dalton Trans.*, 2007, 535–549.
- 50 C. F. Baes, Jr. and R. E. Mesmer, *The Hydrolysis of Cations*, Wiley, New York, 1976.
- 51 M. Kývala and I. Lukeš, International Conference, Chemometrics ×95, Abstract book p. 63, Pardubice (Czech Republic), 1995; full version of TMOPIUM is available (free of charge) on <https://www.natur.cuni.cz/~kyvala/opium.html>.
- 52 M. Meyer, V. Dahaoui-Ginderey, C. Lecomte and R. Guillard, *Coord. Chem. Rev.*, 1998, **178–180**, 1313–1405.
- 53 P. Hermann, J. Kotek and V. Kubíček, *Comprehensive Heterocyclic Chemistry*, ed. D. StC. Black, J. Cossy and C. V. Stevens, Elsevier, 2022. Vol. 14, ch. 14.11, pp. 591–683.
- 54 B. Bosnich, C. K. Poon and M. L. Tobe, *Inorg. Chem.*, 1965, **4**, 1102–1108.
- 55 A. W. Addison, T. N. Rao, J. Reedijk, J. van Rijn and G. C. Verschoor, *J. Chem. Soc., Dalton Trans.*, 1984, 1349–1356.
- 56 J. Kotek, P. Vojtíšek, I. Císařová, P. Hermann and I. Lukeš, *Collect. Czech. Chem. Commun.*, 2001, **66**, 363–381.
- 57 M. M. Le Roy, S. Héry, N. Saffon-Merceron, C. Platas-Iglesias, T. Troadec and R. Tripier, *Inorg. Chem.*, 2023, **62**, 8112–8122.
- 58 J. Kotek, P. Vojtíšek, I. Císařová, P. Hermann, P. Jurečka, J. Rohovec and I. Lukeš, *Collect. Czech. Chem. Commun.*, 2000, **65**, 1289–1316.
- 59 I. Lukeš, J. Kotek, P. Vojtíšek and P. Hermann, *Coord. Chem. Rev.*, 2001, **216–217**, 287–312.
- 60 R. D. Hancock, R. J. Motekaitis, J. Mashishi, I. Cukrowski, J. H. Reibenspies and A. E. Martell, *J. Chem. Soc., Perkin Trans. 2*, 1996, 1925–1929.
- 61 X. Liang and P. J. Sadler, *Chem. Soc. Rev.*, 2004, **33**, 246–266.
- 62 T. J. Clough, L. Jiang, K.-L. Wong and N. J. Long, *Nat. Commun.*, 2019, **10**, 1420.
- 63 K. H. Chalmers, A. M. Kenwright, D. Parker and A. M. Blamire, *Magn. Reson. Med.*, 2011, **66**, 931–936.
- 64 F. Schmid, C. Hölte, D. Parker and C. Faber, *Magn. Reson. Med.*, 2013, **69**, 1056–1062.

